Journal of Computational Physics 463 (2022) 111278

Contents lists available at ScienceDirect

Journal of Computational Physics

www.elsevier.com/locate/jcp

Energy conserving discontinuous Galerkin method with scalar auxiliary variable technique for the nonlinear Dirac equation ☆

Ruize Yang, Yulong Xing *

Department of Mathematics, The Ohio State University, Columbus, OH 43210, USA

ARTICLE INFO

Article history:
Received 11 November 2021
Received in revised form 19 April 2022
Accepted 3 May 2022
Available online 6 May 2022

Keywords:
Dirac equation
Scalar auxiliary variable
Discontinuous Galerkin method
Charge conservation
Global energy conservation

ABSTRACT

In this paper, we propose a fully-discrete energy-conserving scheme for the nonlinear Dirac equation, by combining the scalar auxiliary variable (SAV) technique with discontinuous Galerkin (DG) discretization. We start by discussing the semi-discrete DG discretization, and show that, with suitable choices of numerical fluxes, the resulting method conserves the charge, energy exactly and preserves the multi-symplectic structure. The optimal error estimate of semi-discrete DG scheme is carried out. We combine it with the energy conserving SAV technique, and demonstrate that the fully-discrete scheme conserves the discrete global energy exactly. Both second order SAV method based on the midpoint rule and its high order extension have been studied. The proposed methods have been tested on some numerical experiments, which confirm the optimal rates of convergence and the energy conserving property. Numerical comparison with energy dissipative DG method is also provided to demonstrate that the numerical error of energy conserving method does not grow significantly in long time simulations.

1. Introduction

The Dirac equation was derived by British physicist Paul Dirac [18] in 1928. It is a relativistic wave equation in particle physics, which describes massive spin-1/2 relativistic fermions in (3+1) space-time dimensions. The original form proposed by Dirac is

$$i\hbar\frac{\partial\psi(x,t)}{\partial t}=\left(\beta mc^2-i\hbar c\sum_{j=1}^{3}\alpha_j\partial_{x_j}\right)\psi(x,t), \tag{1.1}$$

where $\psi=\psi(x,t)\in\mathbb{C}^4$ is the wave function for the electron of rest mass m with space-time coordinates (x,t), $i=\sqrt{-1}$ is the imaginary unit, c is the speed of light, and $\hbar$ is the reduced Planck constant. In Planck units, the equation (1.1) can be written as

$$i\partial_t\psi(x,t)=\left(\beta m-i\sum_{j=1}^{3}\alpha_j\partial_{x_j}\right)\psi(x,t). \tag{1.2}$$

☆ The work of this author was partially supported by the NSF grant DMS-1753581.
* Corresponding author.
E-mail addresses: yang.4097@osu.edu (R. Yang), xing.205@osu.edu (Y. Xing).

https://doi.org/10.1016/j.jcp.2022.111278
0021-9991/

Here the 4×4 matrices α_j $(j = 1, 2, 3)$ and β are all Hermitian and they satisfy

$$\{\alpha_j, \alpha_k\} = 2\delta_{jk} I_4, \quad \{\alpha_j, \beta\} = 0, \quad \beta^2 = I_4, \tag{1.3}$$

in which $\{A, B\} := AB + BA$ is the anticommutator. According to the Dirac–Pauli theorem [50, Lemma 2.25], different choices of the matrices α_j and β are equivalent as long as they satisfy (1.3). The most common choice, known as the Dirac–Pauli representation, is

$$\alpha_j = \begin{pmatrix} 0 & \sigma_j \\ \sigma_j & 0 \end{pmatrix}, \quad \beta = \begin{pmatrix} I_2 & 0 \\ 0 & -I_2 \end{pmatrix},$$

where σ_j are the Pauli matrices given by

$$\sigma_1 = \begin{pmatrix} 0 & 1 \\ 1 & 0 \end{pmatrix}, \quad \sigma_2 = \begin{pmatrix} 0 & -i \\ i & 0 \end{pmatrix}, \quad \sigma_3 = \begin{pmatrix} 1 & 0 \\ 0 & -1 \end{pmatrix}.$$

In 1938, Russian physicist Dmitri Ivanenko proposed a nonlinear model of self-interacting electrons by adding a nonlinear term to the Dirac equation. In 1970, Spanish physicist Mario Soler re-introduced and investigated this model in [47], which is now known as the Soler Model:

$$i\partial_t \psi = -i \sum_{j=1}^{3} \alpha_j \partial_{x_j} \psi + (m - f(\psi^* \beta \psi))\beta \psi, \tag{1.4}$$

where ψ^* is the complex conjugate of ψ and f is a real function in $C(\mathbb{R})$ with $f(0) = 0$.

Dirac equation plays a key role in quantum field theory. The analyses of Dirac model (such as well-posedness, stability, existence of local solutions) become challenging due to the unboundedness of the corresponding Hamiltonian functional. There are a number of works [8,35,41,54] on the local and global well-posedness of Cauchy problem for the nonlinear Dirac (NLD) equations, including Thirring model, Federbusch model, Gross–Neveu model and other Dirac equation with quadratic nonlinearity. Particular attention is being paid to the solitary wave dynamics of nonlinear Dirac equations. The first stability result appears in [5] in the context of self-interacting spinor fields, but the stability of solitary wave solutions of the NLD equation has not been settled yet. Recently, Shao et al. studied the stability of solitary waves by numerical simulations in [42]. The behavior of the solitary wave in the presence of external forces was also described in [38,39]. For the (1+1)-dimensional NLD equation (i.e., one time dimension plus one space dimension), some analytical solitary wave solutions are found in [9,27] for the quadric nonlinearity as well as in [36] for fractional nonlinearity while there are few exact solutions in (3+1) dimensions except for some special cases [51].

As the exact solution of nonlinear equations is generally unknown, numerical experiment becomes an important approach. We will henceforth focus on numerical methods of the (1+1)-dimensional NLD equation. Along this direction, Alvarez and Carreras [1,2] made important progress and used a second-order Crank–Nicholson (CN) scheme to simulate the interaction dynamics between two solitary waves of different initial charges for the Soler model. Shao and Tang reinvestigated this interaction dynamics problem in [44] by applying a fourth-order Runge-Kutta discontinuous Galerkin method. With the choice of upwind numerical fluxes, the charge non-increasing property was proved for the semi-discrete DG spatial discretization, and extensive numerical experiments were carried out to demonstrate the performance of the high order DG methods. The weak inelastic interaction in ternary collisions was also observed. In [24], Hong and Li applied the implicit multi-symplectic Runge–Kutta methods (MSRK) to the NLD equation which was rewritten in the form of multi-symplectic Hamiltonian partial differential equation (HPDE) systems. It was shown that the resulting methods preserve exactly the charge and momentum, and the error of the energy is at the level of numerical truncation error. A parallel numerical method for the time-dependent Dirac equation was presented in [19] and a time- and space-staggered leap-frog scheme was proposed in [23]. A comprehensive review of numerical methods for the NLD equation has been studied in [52]. Recently the time-splitting method [3,29], which satisfied the charge conservation in the discrete level, was investigated.

Discontinuous Galerkin (DG) spatial discretization will be considered in this paper. DG methods were first proposed and analyzed in the early 1970s as a finite element method to numerically solve PDEs. They adopt piecewise continuous polynomial space for numerical solutions and test functions in the spatial variables and have been successfully applied to a wide range of problems. They were successfully applied to hyperbolic conservation laws following a series of papers by Cockburn et al. [13–17]. Recently, there have been extensive studies on structure-preserving DG methods which were designed to preserve certain structure of the continuum equations, such as the total energy, Hamiltonian structure, the physical bounds, asymptotic limit, hydrostatic balance, and entropy inequality. For instance, energy or Hamiltonian conserving DG methods, with smaller phase and shape errors in long time simulations, have been designed and studied for the acoustic wave [11], the elastodynamics [22], the generalized Korteweg-de Vries equation [4,32], the Camassa-Holm equation [31], the Degasperis-Procesi equation [26], and the nonlinear Schrödinger equation [30]. The multi-symplecticity of semi-discrete DG discretization have been studied for general multi-symplectic HPDEs in a recent paper [48]. Recent development on efficient energy stable or energy conserving temporal discretizations includes the invariant energy quadratization (IEQ) approach [7,53] and the scalar auxiliary variable (SAV) method [46], which can be proven to be energy stable/conserving while avoiding solving the implicit complicated nonlinear system. The IEQ approach was introduced in [55] and its high order version

was recently discussed in [20,34]. Shen and Xu performed the convergence and error analysis of SAV method in [45] and optimal error estimates for the SAV finite-elements schemes were derived in [10]. The SAV method can be extended to high order method in time while being unconditionally energy stable [21]. Recently a new variant of SAV approach for gradient flows was proposed in [25].

In this paper, we propose fully-discrete energy-conserving numerical methods for solving the (1+1)-dimensional NLD equation, by combining the efficient SAV time discretization and energy-conserving DG methods. We start by discussing the semi-discrete DG spatial discretization, and show that, with suitable choices of numerical fluxes, the resulting method is able to conserve the charge and energy exactly in the discrete level. In addition, one can rewrite the NLD equation into the HPDE form, and show that the semi-discrete DG method can preserve the multi-symplectic structure. The optimal error estimate of semi-discrete DG scheme is also studied, by introducing a novel global projection following the recent study in [49]. The semi-discrete method could be coupled with various energy conserving time discretization. To avoid solving the nonlinear system at each time step, we choose the energy conserving SAV method, and denote the resulting fully-discrete scheme by SAV-DG method. We start with the second order SAV method derived from the midpoint rule, and provide an efficient way to implement this method so that only one linear system needs to be solved at each time step. The fully-discrete SAV-DG scheme is shown to conserve the discrete global energy exactly. The extension to fourth order energy conserving SAV method is also studied in the paper, and its implementation is simple, as we can just use the second order algorithm and iterate it three times to obtain higher order. The proposed methods have been tested on various numerical experiments, which demonstrate the optimal convergence rate as well as the energy conserving property. We also carry out the comparison of numerical errors of energy conserving DG method and energy dissipative DG method (with upwind fluxes), and it was observed that energy conserving method yields a much smaller numerical error in a long time simulation.

The rest of the paper is organized as follows. In Section 2, we write the (1+1)-dimensional NLD equation in the form of HPDE system, and present its exact solitary wave solutions. In Section 3, we apply DG method to the HPDE system and show that the semi-discrete scheme conserves the charge and energy exactly with suitable choices of numerical fluxes. The error estimate of semi-discrete DG discretization is given in Section 4. In section 5, we construct the SAV-DG method along with its higher order version and present the discrete global energy conservation law of the method. Numerical examples are illustrated in Section 6 to verify the accuracy of our scheme and demonstrate the long time behavior of SAV-DG methods for NLD equation. We finish with a concluding remark in Section 7.

2. Preliminaries

In this study, we restrict our attention to (1+1)-dimensional nonlinear Dirac equation of the form

$$
\begin{aligned}
&i\partial_t\psi = -i\alpha\partial_x\psi + (m - f(\psi^*\beta\psi))\beta\psi,\\
&\psi(x,0) = (\phi_1(x),\ \phi_2(x))^{\mathrm{T}},
\end{aligned}
$$

where $\psi = (\psi_1, \psi_2)^{\mathrm{T}}$ is a spinorial wave function, with ψ_1 and ψ_2 being complex functions that describe the up and down states of the particle. We choose $\alpha = \sigma_1$, $\beta = \sigma_3$ and $f(s) = 2\lambda s$ as in [44] with λ being a real constant. This leads to the PDE system

$$
\begin{aligned}
&\partial_t\psi_1 + \partial_x\psi_2 + im\psi_1 + 2i\lambda\left(|\psi_2|^2 - |\psi_1|^2\right)\psi_1 = 0,\\
&\partial_t\psi_2 + \partial_x\psi_1 - im\psi_2 + 2i\lambda\left(|\psi_1|^2 - |\psi_2|^2\right)\psi_2 = 0.
\end{aligned}
\tag{2.1}
$$

The NLD equations admit three conserved quantities: the energy $E(t)$, the linear momentum $P(t)$, and the charge $Q(t)$, given by

$$
\begin{aligned}
E(t) = -\frac{1}{2}\int_{\mathbb{R}} \mathrm{d}x\Big[&\mathrm{Im}\left(\psi_1^*\partial_x\psi_2 + \psi_2^*\partial_x\psi_1\right) + m\left(|\psi_1|^2 - |\psi_2|^2\right)\\
&-\lambda\left(|\psi_1|^2 - |\psi_2|^2\right)^2\Big] =: \int_{\mathbb{R}} \mathrm{d}x\rho_E(x,t),
\end{aligned}
\tag{2.2}
$$

$$
P(t) = \frac{1}{2}\int_{\mathbb{R}} \mathrm{d}x\left[\mathrm{Im}\left(\psi_1^*\partial_x\psi_1 + \psi_2^*\partial_x\psi_2\right)\right] =: \int_{\mathbb{R}} \mathrm{d}x\rho_P(x,t),
\tag{2.3}
$$

$$
Q(t) = \int_{\mathbb{R}} \mathrm{d}x\left(|\psi_1|^2 + |\psi_2|^2\right) =: \int_{\mathbb{R}} \mathrm{d}x\rho_Q(x,t),
\tag{2.4}
$$

where ρ_E, ρ_P, and ρ_Q represent the energy density, the linear momentum density, and the charge density respectively.

By considering the real and imaginary parts of the unknown variables as $\psi_1 = p_1 + iq_1$, $\psi_2 = p_2 + iq_2$, the NLD equations (2.1) can be rewritten in the following form

$$\frac{\partial p_1}{\partial t}+\frac{\partial p_2}{\partial x}-mq_1-2\lambda\left(p_2^2+q_2^2-p_1^2-q_1^2\right)q_1=0,$$
$$\frac{\partial q_1}{\partial t}+\frac{\partial q_2}{\partial x}+mp_1+2\lambda\left(p_2^2+q_2^2-p_1^2-q_1^2\right)p_1=0,$$
$$\frac{\partial p_2}{\partial t}+\frac{\partial p_1}{\partial x}+mq_2+2\lambda\left(p_2^2+q_2^2-p_1^2-q_1^2\right)q_2=0,$$
$$\frac{\partial q_2}{\partial t}+\frac{\partial q_1}{\partial x}-mp_2-2\lambda\left(p_2^2+q_2^2-p_1^2-q_1^2\right)p_2=0.$$

The above system can be reorganized as a multi-symplectic HPDE system, which has a multi-symplectic structure of the form

$$M\boldsymbol{z}_t+K\boldsymbol{z}_x=\nabla_z S(\boldsymbol{z}), \tag{2.5}$$

with the real-valued state variable $\boldsymbol{z}=(p_1,q_1,p_2,q_2)^{\mathrm{T}}$. The matrices M and K are skew-symmetric:

$$M=\begin{pmatrix}0&1&0&0\\-1&0&0&0\\0&0&0&1\\0&0&-1&0\end{pmatrix},\quad K=\begin{pmatrix}0&0&0&1\\0&0&-1&0\\0&1&0&0\\-1&0&0&0\end{pmatrix}, \tag{2.6}$$

and $S:R^4\to R$ is a smooth function

$$\begin{aligned}S(\boldsymbol{z})=&\frac{1}{2}\left(\lambda\left(p_1^2+q_1^2-p_2^2-q_2^2\right)-m\right)\left(p_1^2+q_1^2-p_2^2-q_2^2\right)\\=&\frac{1}{2}\lambda\left(p_1^2+q_1^2-p_2^2-q_2^2\right)^2-\frac{1}{2}m\left(p_1^2+q_1^2-p_2^2-q_2^2\right).\end{aligned} \tag{2.7}$$

As an HPDE system, it admits the multi-symplectic conservation law [6]

$$\omega_t+\kappa_x=0,\qquad \text{with}\quad \omega=M\boldsymbol{z}_1\cdot\boldsymbol{z}_2,\quad \kappa=K\boldsymbol{z}_1\cdot\boldsymbol{z}_2,$$

where $\boldsymbol{z}_1$ and $\boldsymbol{z}_2$ are any pair of solutions of the variational equation of (2.5) of the form

$$M(d\boldsymbol{z})_t+K(d\boldsymbol{z})_x=\nabla_{\boldsymbol{zz}}S(\boldsymbol{z})d\boldsymbol{z}.$$

Remark 2.1. The exact solutions of the NLD equations (2.1) can be found in some cases. The first one is a standing wave solution at x_0:

$$\psi_1^{sw}(x-x_0,t)=A(x-x_0)e^{-i\Lambda t}, \tag{2.8a}$$
$$\psi_2^{sw}(x-x_0,t)=iB(x-x_0)e^{-i\Lambda t}, \tag{2.8b}$$

where

$$A(x)=\frac{\sqrt{(m^2-\Lambda^2)(m+\Lambda)/\lambda}\cosh\sqrt{m^2-\Lambda^2}x}{m+\Lambda\cosh 2\sqrt{m^2-\Lambda^2}x},$$
$$B(x)=\frac{\sqrt{(m^2-\Lambda^2)(m-\Lambda)/\lambda}\sinh\sqrt{m^2-\Lambda^2}x}{m+\Lambda\cosh 2\sqrt{m^2-\Lambda^2}x},$$

with $0<\Lambda\leqslant m$. They also admit single solitary traveling wave exact solutions, placed initially at x_0 with a velocity v:

$$\psi_1^{ss}(x-x_0,t)=\sqrt{\frac{\gamma+1}{2}}\psi_1^{sw}(\tilde{x},\tilde{t})+\mathrm{sgn}(v)\sqrt{\frac{\gamma-1}{2}}\psi_2^{sw}(\tilde{x},\tilde{t}), \tag{2.9a}$$
$$\psi_2^{ss}(x-x_0,t)=\mathrm{sgn}(v)\sqrt{\frac{\gamma-1}{2}}\psi_1^{sw}(\tilde{x},\tilde{t})+\sqrt{\frac{\gamma+1}{2}}\psi_2^{sw}(\tilde{x},\tilde{t}), \tag{2.9b}$$

where $\gamma=1/\sqrt{1-v^2}$, $\tilde{x}=\gamma(x-x_0-vt)$, $\tilde{t}=\gamma[t-v(x-x_0)]$. The shape of solitary wave solution (2.9) depends on the parameter Λ. When $0<\Lambda<m/2$, it is a two-hump soliton; when $m/2\leqslant\Lambda<m$, it is a one-hump soliton; when $\Lambda=m$, the wave vanishes. The single solitary wave solution reduces to the standing wave solution if $v=0$.

3. Semi-discrete discontinuous Galerkin method

Suppose that the spatial domain Ω can be discretized as $\Omega = \cup_{j=1}^{N} I_j$, where $I_j = [x_{j-\frac{1}{2}}, x_{j+\frac{1}{2}}]$ for $j = 1, 2, ..., N$. We denote by Δx_j the length of I_j and by $h = \Delta x = \max_j \Delta x_j$ the maximum mesh size. The computational meshes are denoted by $\mathcal{T}_h$. We use $P^k(I_j)$ to represent the vector space spanned by polynomials of degrees up to k on the element I_j, and define

$$V_h = \left\{ v \in L^2(\Omega) : v|_{I_j} \in P^k(I_j),\ j = 1, 2, ...N \right\}$$

to be the discontinuous piecewise polynomial space. We denote by $\boldsymbol{V}_h = \Pi_{i=1}^{4} V_h$ the space of finite element numerical solutions. For any piecewise polynomial $v \in V_h$ or $\boldsymbol{V}_h$, let $v^+_{j+1/2}$ and $v^-_{j+1/2}$ be the limit at the cell interface $x_{j+1/2}$ from the right and left cells respectively, and define the average and jump of v at the cell interface $x_{j+1/2}$ as

$$\{v\}_{j+\frac{1}{2}} = \frac{1}{2}(v^+_{j+\frac{1}{2}} + v^-_{j+\frac{1}{2}}), \quad [v]_{j+\frac{1}{2}} = v^+_{j+\frac{1}{2}} - v^-_{j+\frac{1}{2}}.$$

We denote by $\|\cdot\|_j$ the L^2 norm over the cell I_j, and $\|\cdot\|$ the L^2 norm over the entire domain Ω.

The semi-discrete DG method of the NLD equations in the HPDE form (2.5) is given as follows: Seek the numerical solutions $\boldsymbol{z}_h \in \boldsymbol{V}_h$ such that

$$\int_{I_j} M(\boldsymbol{z}_h)_t \cdot \boldsymbol{\phi} dx - \int_{I_j} K\boldsymbol{z}_h \cdot \boldsymbol{\phi}_x dx + \left(\widehat{K\boldsymbol{z}_h} \cdot \boldsymbol{\phi}^-\right)_{j+\frac{1}{2}} - \left(\widehat{K\boldsymbol{z}_h} \cdot \boldsymbol{\phi}^+\right)_{j-\frac{1}{2}} = \int_{I_j} \nabla_{\boldsymbol{z}} S(\boldsymbol{z}_h) \cdot \boldsymbol{\phi} dx, \tag{3.1}$$

holds for all test functions $\boldsymbol{\phi} \in \boldsymbol{V}_h$. The hatted terms $\widehat{K\boldsymbol{z}_h}$ are the numerical fluxes defined on the element interfaces, and are the key component in designing stable DG methods. We consider the family of the numerical flux

$$\widehat{K\boldsymbol{z}_h} = K\{\boldsymbol{z}_h\} + A[\boldsymbol{z}_h], \tag{3.2}$$

for any $m \times m$ real symmetric matrix A. A slightly different version of this numerical flux was also considered in [48] for DG methods applied to HPDE.

For certain choices of A in the numerical flux (3.2), we can achieve the exact conservation of the charge $Q(t)$ defined in (2.4), as summarized below.

Proposition 3.1 (***Charge conservation***). *Assume $\boldsymbol{z}_h = (p_1, q_1, p_2, q_2)^{\mathrm{T}}$ is the numerical solution of the semi-discrete DG method (3.1) with the numerical flux (3.2), where the symmetric matrix A takes the form*

$$A = (a_{ij}) = \begin{pmatrix} a_1 & 0 & a_3 & a_4 \\ 0 & a_1 & -a_4 & a_3 \\ a_3 & -a_4 & a_2 & 0 \\ a_4 & a_3 & 0 & a_2 \end{pmatrix}. \tag{3.3}$$

Define $Q_h(t) = \int_\Omega \left(p_{1,h}^2 + p_{2,h}^2 + q_{1,h}^2 + q_{2,h}^2\right) dx$ and $Q_{h,j}(t) = \int_{I_j} \left(p_{1,h}^2 + p_{2,h}^2 + q_{1,h}^2 + q_{2,h}^2\right) dx$ to be the global and local charge. There holds the local charge conservation of the form:

$$\frac{dQ_{h,j}(t)}{dt} + \mathcal{G}(\boldsymbol{z}_h)_{j+\frac{1}{2}} - \mathcal{G}(\boldsymbol{z}_h)_{j-\frac{1}{2}} = 0, \tag{3.4}$$

where

$$\begin{aligned} \mathcal{G}(\boldsymbol{z}_h) :=& \frac{1}{2}\mu^+(p_{1,h}, p_{2,h}) + \frac{1}{2}\mu^+(q_{1,h}, q_{2,h}) + a_1\mu^-(p_{1,h}, q_{1,h}) + a_2\mu^-(p_{2,h}, q_{2,h}) \\ &+ a_3(\mu^-(p_{1,h}, q_{2,h}) + \mu^-(p_{2,h}, q_{1,h})) + a_4(\mu^-(p_{2,h}, p_{1,h}) + \mu^-(q_{2,h}, q_{1,h})), \end{aligned} \tag{3.5}$$

and $\mu^{\pm}(u_h, v_h) = u_h^+ v_h^- \pm u_h^- v_h^+$. Furthermore, we have the global conservation of the charge:

$$\frac{dQ_h(t)}{dt} = \frac{d}{dt} \int_\Omega \left(p_{1,h}^2 + p_{2,h}^2 + q_{1,h}^2 + q_{2,h}^2\right) dx = 0. \tag{3.6}$$

Proof. Taking the test function $\boldsymbol{\phi} = M\boldsymbol{z}_h$ in (3.1), we have

$$\int_{I_j} M(\boldsymbol{z}_h)_t \cdot M\boldsymbol{z}_h dx - \int_{I_j} K\boldsymbol{z}_h \cdot M\boldsymbol{z}_{hx} dx + \left(\widehat{K\boldsymbol{z}_h} \cdot M\boldsymbol{z}_h^-\right)_{j+\frac{1}{2}} - \left(\widehat{K\boldsymbol{z}_h} \cdot M\boldsymbol{z}_h^+\right)_{j-\frac{1}{2}} = \int_{I_j} \nabla_{\boldsymbol{z}} S(\boldsymbol{z}_h) \cdot M\boldsymbol{z}_h dx.$$

First of all, it can be shown that the right-hand side disappears, i.e., $\int_{I_j} \nabla_{\boldsymbol{z}} S(\boldsymbol{z}_h) \cdot M\boldsymbol{z}_h dx = 0$, which follows directly from the definition of $S(\boldsymbol{z}_h)$ in (2.7) and M in (2.6). Next, the volume integral becomes

$$\begin{aligned} -\int_{I_j} K\boldsymbol{z}_h \cdot M\boldsymbol{z}_{hx} dx &= -\int_{I_j} \left(q_{2,h}(q_{1,h})_x + p_{2,h}(p_{1,h})_x + q_{1,h}(q_{2,h})_x + p_{1,h}(p_{2,h})_x\right) dx \\ &= -\left(p_{1,h}p_{2,h} + q_{1,h}q_{2,h}\right)\Big|_{x^+_{j-\frac{1}{2}}}^{x^-_{j+\frac{1}{2}}}, \end{aligned}$$

with M, K defined in (2.6). Therefore, we have

$$\frac{dQ_{h,j}(t)}{dt} + \left(K\{\boldsymbol{z}_h\} \cdot M\boldsymbol{z}_h - p_{1,h}p_{2,h} - q_{1,h}q_{2,h} + A[\boldsymbol{z}_h] \cdot M\boldsymbol{z}_h\right)\Big|_{x^+_{j-\frac{1}{2}}}^{x^-_{j+\frac{1}{2}}} = 0, \tag{3.7}$$

by utilizing the fact that $\int_{I_j} M(\boldsymbol{z}_h)_t \cdot M\boldsymbol{z}_h dx = dQ_{h,j}(t)/dt$.

Straightforward computation leads to

$$\begin{aligned} & K\{\boldsymbol{z}_h\} \cdot (M\boldsymbol{z}_h^-)_{j+\frac{1}{2}} - (p_{1,h}p_{2,h} + q_{1,h}q_{2,h})^-_{j+\frac{1}{2}} \\ =\ & \left(\{q_{2,h}\}q^-_{1,h} + \{p_{2,h}\}p^-_{1,h} + \{q_{1,h}\}q^-_{2,h} + \{p_{1,h}\}p^-_{2,h}\right)_{j+\frac{1}{2}} - (p_{1,h}p_{2,h} + q_{1,h}q_{2,h})^-_{j+\frac{1}{2}} \\ =\ & \left(\frac{1}{2}\mu^+(p_{1,h}, p_{2,h}) + \frac{1}{2}\mu^+(q_{1,h}, q_{2,h})\right)_{j+\frac{1}{2}}, \end{aligned}$$

and

$$\begin{aligned} A[\boldsymbol{z}_h] \cdot (M\boldsymbol{z}_h^-)_{j+\frac{1}{2}} = \Big[& a_1\mu^-(p_{1,h}, q_{1,h}) + a_2\mu^-(p_{2,h}, q_{2,h}) \\ & + a_3(\mu^-(p_{1,h}, q_{2,h}) + \mu^-(p_{2,h}, q_{1,h})) + a_4(\mu^-(p_{2,h}, p_{1,h}) + \mu^-(q_{2,h}, q_{1,h}))\Big]_{j+\frac{1}{2}}. \end{aligned}$$

Hence, we have

$$K\{\boldsymbol{z}_h\} \cdot (M\boldsymbol{z}_h^-)_{j+\frac{1}{2}} - (p_{1,h}p_{2,h} + q_{1,h}q_{2,h})^-_{j+\frac{1}{2}} + A[\boldsymbol{z}_h] \cdot (M\boldsymbol{z}_h^-)_{j+\frac{1}{2}} = \mathcal{G}(\boldsymbol{z}_h)_{j+\frac{1}{2}},$$

and similarly

$$K\{\boldsymbol{z}_h\} \cdot (M\boldsymbol{z}_h^+)_{j-\frac{1}{2}} - (p_{1,h}p_{2,h} + q_{1,h}q_{2,h})^+_{j-\frac{1}{2}} + A[\boldsymbol{z}_h] \cdot (M\boldsymbol{z}_h^+)_{j-\frac{1}{2}} = \mathcal{G}(\boldsymbol{z}_h)_{j-\frac{1}{2}}.$$

Combining these with (3.7) leads to the local conservation of charge in (3.4). The global conservation of charge (3.6) can be obtained by summing (3.4) over all elements and using the periodic boundary condition. □

In [48], semi-discrete DG methods with suitable choices of numerical fluxes for the HPDEs are shown to be both multi-symplectic and energy conserving. The result on energy conservation is summarized below for the NLD equations, and we refer to [48] for the result on the preservation of multi-symplectic structure by the proposed semi-discrete DG method (3.1).

Proposition 3.2 (***Energy conservation***). *Let $\boldsymbol{z}_h$ be the numerical solution of the semi-discrete DG scheme (3.1). It satisfies the local energy conservation law in the form of*

$$\frac{d\mathcal{E}_{h,j}}{dt} + \frac{1}{2}\mathcal{F}(\boldsymbol{z}_h, (\boldsymbol{z}_h)_t)_{j+\frac{1}{2}} - \frac{1}{2}\mathcal{F}(\boldsymbol{z}_h, (\boldsymbol{z}_h)_t)_{j-\frac{1}{2}} = 0,$$

where $\mathcal{E}_{h,j} = \int_{I_j} \rho_E(\boldsymbol{z}_h)dx - \frac{1}{2}\widehat{K\boldsymbol{z}_h} \cdot \boldsymbol{z}_h^- + \frac{1}{2}\widehat{K\boldsymbol{z}_h} \cdot \boldsymbol{z}_h^+$ with

$$\begin{aligned} \rho_E(\boldsymbol{z}_h) = S(\boldsymbol{z}_h) - \frac{1}{2}K(\boldsymbol{z}_h)_x \cdot \boldsymbol{z}_h = & \frac{\lambda}{2}\left(p_{1,h}^2 + q_{1,h}^2 - p_{2,h}^2 - q_{2,h}^2\right)^2 - \frac{m}{2}\left(p_{1,h}^2 + q_{1,h}^2 - p_{2,h}^2 - q_{2,h}^2\right) \\ & - \frac{1}{2}((q_{2,h})_x p_{1,h} - (p_{2,h})_x q_{1,h} + (q_{1,h})_x p_{2,h} - (p_{1,h})_x q_{2,h}). \end{aligned}$$

This leads to the conservation of the total energy

$$\mathcal{E}_h = \int_\Omega \rho_E(\boldsymbol{z}_h)dx + \frac{1}{2}\sum_j \left((K\{\boldsymbol{z}_h\} + A[\boldsymbol{z}_h]) \cdot [\boldsymbol{z}_h]\right)_{j+\frac{1}{2}}. \tag{3.8}$$

Remark 3.1. The conserved total energy (3.8) contains some boundary terms, and can be simplified for specific matrix A. Below, let us use the alternating fluxes as an example to illustrate it. We notice that a special choice of A given by

$$A = \begin{pmatrix} 0 & 0 & 0 & \frac{1}{2} \\ 0 & 0 & -\frac{1}{2} & 0 \\ 0 & -\frac{1}{2} & 0 & 0 \\ \frac{1}{2} & 0 & 0 & 0 \end{pmatrix},$$

corresponds to the alternating flux, i.e., $\hat{q}_{2,h} = q^+_{2,h}$, $\hat{p}_{2,h} = p^+_{2,h}$, $\hat{q}_{1,h} = q^-_{1,h}$, and $\hat{p}_{1,h} = p^-_{1,h}$. We can define a bilinear form $D^\pm_h : H^1(\mathcal{T}_h) \times H^1(\mathcal{T}_h) \to \mathbb{R}$ as

$$D^\pm_h(v, w) = -\int_\Omega v w_x dx - \sum_j \left(\{v\}[w] \pm \frac{1}{2}[v][w] \right)_{j+\frac{1}{2}} = -\int_\Omega v w_x dx - \sum_j \left(v^\pm [w] \right)_{j+\frac{1}{2}},$$

which approximates the term $\int_\Omega v_x w dx$ in the following sense: for all $v \in C^1(I)$, there holds

$$D^\pm_h(v, w) = \int_\Omega v_x w dx, \qquad \forall w \in H^1(\mathcal{T}_h).$$

Using the Riesz Representation Theorem, we can define the numerical derivative operator $D^\pm_h : H^1(\mathcal{T}_h) \to V_h$ via

$$(D^\pm_h v, w) = D^\pm_h(v, w), \qquad \forall w \in V_h.$$

With the new notations, one can show that the discrete total energy (3.8) can be rewritten as

$$\begin{aligned} \mathcal{E}_h = &\int_\Omega \frac{\lambda}{2} \left(p^2_{1,h} + q^2_{1,h} - p^2_{2,h} - q^2_{2,h} \right)^2 - \frac{m}{2} \left(p^2_{1,h} + q^2_{1,h} - p^2_{2,h} - q^2_{2,h} \right) dx \\ &- \frac{1}{2} \big((D^+_h q_{2,h},\ p_{1,h}) - (D^+_h p_{2,h},\ q_{1,h}) + (D^-_h q_{1,h},\ p_{2,h}) - (D^-_h p_{1,h},\ q_{2,h}) \big), \end{aligned}$$

which is a numerical approximation to the continuous total energy

$$\mathcal{E} = \frac{1}{2} \int_\Omega \lambda \left(p^2_1 + q^2_1 - p^2_2 - q^2_2 \right)^2 - m \left(p^2_1 + q^2_1 - p^2_2 - q^2_2 \right) - \big((q_2)_x p_1 - (p_2)_x q_1 + (q_1)_x p_2 - (p_1)_x q_2 \big) \, dx.$$

In addition, this matrix A satisfies the form (3.3) with $a_1 = a_2 = a_3 = 0$ and $a_4 = \pm 1/2$. Therefore, the semi-discrete DG method (3.1) with the alternating fluxes conserves the charge and the energy simultaneously.

4. Error estimate

We will provide optimal error estimate analysis of the semi-discrete DG scheme (3.1) in this section. Throughout the paper, the numerical flux $\widehat{K\boldsymbol{z}_h} = K\{\boldsymbol{z}_h\} + A[\boldsymbol{z}_h]$ with A given in (3.3) will be used, such that the resulting semi-discrete DG method enjoys the charge conservation, multi-symplecticity and energy conservation properties simultaneously.

4.1. Projection properties

We start by reviewing some existing results on the projection and their error analysis. For a given smooth function u, we can define its Gauss-Radau projection Pu into the space V_h as

$$\int_{I_j} (Pu - u) w = 0, \quad \forall w \in P^{k-1}(I_j); \quad Pu(x^-_{j+\frac{1}{2}}) = u(x_{j+\frac{1}{2}}),$$

on each cell I_j. It is known that the projection Pu is well defined and has the projection error [12]

$$\|Pu - u\| \leqslant Ch^{k+1}, \qquad \|Pu - u\|_\infty \leqslant Ch^k, \tag{4.1}$$

with $C = C(\|u\|_{H^{k+1}})$ independent of h. The same error estimate holds if the condition $Pu(x^-_{j+\frac{1}{2}}) = u(x_{j+\frac{1}{2}})$ is replaced by $Pu(x^+_{j-\frac{1}{2}}) = u(x_{j-\frac{1}{2}})$. In addition, the generalized Gauss-Radau projection P^λ was discussed in [37], which was defined as

$$\int_{I_j} (P^\lambda u - u) w = 0, \quad \forall w \in P^{k-1}(I_j),$$
$$\{P^\lambda u\} + \lambda [P^\lambda u] = u, \quad \text{at } x = x_{j+\frac{1}{2}},$$

with $\lambda \neq 0$ for all the elements I_j. It was shown to yield optimal approximation error. Based on these, we present the following lemma on the projection to be used in the proof of main result.

Lemma 4.1. *Suppose $\boldsymbol{z} : \mathbb{R} \to \mathbb{R}^4$ is a smooth vector-valued function. For the numerical fluxes defined in (3.2) with the entries of the matrix A in (3.3) satisfying $a_1 a_2 - a_3^2 - a_4^2 \neq 0$, there exists a projection P such that*

$$\int_{I_j} (P\boldsymbol{z} - \boldsymbol{z}) \cdot \boldsymbol{\phi}_h = 0, \quad \forall \boldsymbol{\phi}_h \in (P^{k-1}(I_j))^4,$$
$$\widehat{K(P\boldsymbol{z})} = \widehat{K\boldsymbol{z}}, \quad \text{at } x = x_{j+\frac{1}{2}}$$

for each j. Furthermore, the following approximation property holds

$$\|\boldsymbol{z} - P\boldsymbol{z}\| \leqslant Ch^{k+1}, \tag{4.2}$$

where C may depend on $\boldsymbol{z}$ and the entries of A but is independent of h.

Under the assumption $a_1 a_2 - a_3^2 - a_4^2 \neq 0$, the matrix A is nonsingular and diagonalizable. This Lemma can be proven following the similar way as that of [49, Lemma 2.1], and is skipped here to save space.

Moreover, we list some inverse properties of the one-dimensional finite element space V_h that will be used. For any piecewise polynomial $v_h \in V_h$, there is a positive constant C independent of v_h and h such that [12]

$$\|(v_h)_x\| \leqslant Ch^{-1} \|v_h\|, \qquad \|v_h\|_\infty \leqslant Ch^{-\frac{1}{2}} \|v_h\|. \tag{4.3}$$

4.2. Error analysis

To deal with the nonlinear source term, we follow the setup in [28] and make an a priori error estimate assumption between numerical solution $\boldsymbol{z}_h$ and exact solution $\boldsymbol{z}$:

$$\|\boldsymbol{z} - \boldsymbol{z}_h\| \leqslant h. \tag{4.4}$$

This estimate, combined with (4.1) and (4.3), implies that

$$\|\boldsymbol{z} - \boldsymbol{z}_h\|_\infty \leqslant \|\boldsymbol{z} - P\boldsymbol{z}\|_\infty + \|P\boldsymbol{z} - \boldsymbol{z}_h\|_\infty \leqslant C(h^k + h^{\frac{1}{2}}) < C, \tag{4.5}$$

when h is small enough. We will verify the assumption (4.4) at the end of the proof of Theorem 4.2. Now we are ready to prove the main result on optimal L^2 error estimate of the semi-discrete DG scheme to the NLD equation.

Theorem 4.2. *let $\boldsymbol{z}$ be an exact solution to the NLD equation (2.1), or equivalently, the HPDE form (2.5) with M, K and S defined in (2.6)-(2.7), which is sufficiently smooth and bounded. Let $\boldsymbol{z}_h \in \boldsymbol{V}_h$ be the solution of the semi-discrete DG scheme (3.1)-(3.2), with the numerical fluxes defined in (3.2)-(3.3) and the entries of the matrix A satisfying $a_1 a_2 - a_3^2 - a_4^2 \neq 0$. Suppose that the initial condition is well chosen such that $\|\boldsymbol{z}(x,0) - \boldsymbol{z}_h(x,0)\| = O(h^{k+1})$. Then for $k \geqslant 1$, there holds the following error estimates*

$$\|\boldsymbol{z} - \boldsymbol{z}_h\| \leqslant Ch^{k+1},$$

where C depends on $\boldsymbol{z}$, and their derivatives but is independent of the mesh size h.

Proof. Let us first introduce some notations by defining a bilinear form

$$B_j(\boldsymbol{z}_h, \boldsymbol{\phi}) = \int_{I_j} M(\boldsymbol{z}_h)_t \cdot \boldsymbol{\phi} dx - \int_{I_j} K\boldsymbol{z}_h \cdot \boldsymbol{\phi}_x dx + \left(\widehat{K\boldsymbol{z}_h} \cdot \boldsymbol{\phi}^-\right)_{j+\frac{1}{2}} - \left(\widehat{K\boldsymbol{z}_h} \cdot \boldsymbol{\phi}^+\right)_{j-\frac{1}{2}},$$

and decomposing the error into two parts as

$$e = \boldsymbol{z} - \boldsymbol{z}_h = \eta + \xi, \quad \xi = P\boldsymbol{z} - \boldsymbol{z}_h, \quad \eta = \boldsymbol{z} - P\boldsymbol{z},$$

where P denotes the projection introduced in Lemma 4.1.

The DG scheme (3.1) can then be written as

$$B_j(\boldsymbol{z}_h, \boldsymbol{\phi}) = \int_{I_j} (\nabla_{\boldsymbol{z}} S)(\boldsymbol{z}_h) \cdot \boldsymbol{\phi} dx$$

for all $\boldsymbol{\phi} \in \boldsymbol{V}_h$. The exact solution $\boldsymbol{z}$ also satisfies the same equation, therefore, the difference of them yields

$$B_j(\boldsymbol{z} - \boldsymbol{z}_h, \boldsymbol{\phi}) = \int_{I_j} [(\nabla_{\boldsymbol{z}} S)(\boldsymbol{z}) - (\nabla_{\boldsymbol{z}} S)(\boldsymbol{z}_h)] \cdot \boldsymbol{\phi} dx,$$

for all $\boldsymbol{\phi} \in \boldsymbol{V}_h$. Taking the test function $\boldsymbol{\phi} = M\xi \in \boldsymbol{V}_h$ leads to

$$B_j(\xi, M\xi) = -B_j(\eta, M\xi) + \int_{I_j} [(\nabla_{\boldsymbol{z}} S)(\boldsymbol{z}) - (\nabla_{\boldsymbol{z}} S)(\boldsymbol{z}_h)] \cdot M\xi dx. \tag{4.6}$$

For the left-hand side of (4.6), we have

$$\begin{aligned} B_j(\xi, M\xi) &= \int_{I_j} M\xi_t \cdot M\xi dx - \int_{I_j} K\xi \cdot M\xi_x dx + \left(\widehat{K\xi} \cdot M\xi^-\right)_{j+\frac{1}{2}} - \left(\widehat{K\xi} \cdot M\xi^+\right)_{j-\frac{1}{2}} \\ &= \frac{1}{2}\frac{d}{dt}\|M\xi\|_j^2 + \hat{F}_{j+\frac{1}{2}} - \hat{F}_{j-\frac{1}{2}} + \Theta_{j-\frac{1}{2}}, \end{aligned}$$

where

$$\begin{aligned} \hat{F}_{j+\frac{1}{2}} &= -\int_{}^{x^-_{j+\frac{1}{2}}} K\xi \cdot M\xi_x dx + \left(\widehat{K\xi}\right)_{j+\frac{1}{2}} \cdot M\xi(x^-_{j+\frac{1}{2}}) \\ \Theta_{j-\frac{1}{2}} &= \int_{x^-_{j-\frac{1}{2}}}^{x^+_{j-\frac{1}{2}}} K\xi \cdot M\xi_x dx - \left(\widehat{K\xi}\right)_{j-\frac{1}{2}} \cdot \left(M\xi(x^+_{j-\frac{1}{2}}) - M\xi(x^-_{j-\frac{1}{2}})\right). \end{aligned}$$

We claim that $\Theta_{j-\frac{1}{2}} = 0$. From the definitions of M, K and A in (2.6), (3.3), one can show that the product $M^T K$ is symmetric and $M^T A$ is skew-symmetric. It follows that $Ku \cdot Mv = Mu \cdot Kv = Kv \cdot Mu$ and $Av \cdot Mv = 0$ for all $u, v \in \mathbb{R}^4$. Therefore,

$$\begin{aligned} \int_{x^-_{j-\frac{1}{2}}}^{x^+_{j-\frac{1}{2}}} K\xi \cdot M\xi_x dx &= \frac{1}{2}\int_{x^-_{j-\frac{1}{2}}}^{x^+_{j-\frac{1}{2}}} (K\xi \cdot M\xi_x + M\xi \cdot K\xi_x) dx = \frac{1}{2}\int_{x^-_{j-\frac{1}{2}}}^{x^+_{j-\frac{1}{2}}} (K\xi \cdot M\xi)_x dx \\ &= \frac{1}{2}\left(K\xi^+_{j-\frac{1}{2}} \cdot M\xi^+_{j-\frac{1}{2}} - K\xi^-_{j-\frac{1}{2}} \cdot M\xi^-_{j-\frac{1}{2}}\right) \\ &= \frac{1}{2}\left(K\xi^+_{j-\frac{1}{2}} \cdot M\xi^+_{j-\frac{1}{2}} + K\xi^-_{j-\frac{1}{2}} \cdot M\xi^+_{j-\frac{1}{2}} - K\xi^+_{j-\frac{1}{2}} \cdot M\xi^-_{j-\frac{1}{2}} - K\xi^-_{j-\frac{1}{2}} \cdot M\xi^-_{j-\frac{1}{2}}\right) \\ &= \frac{1}{2}K(\xi^+_{j-\frac{1}{2}} + \xi^-_{j-\frac{1}{2}}) \cdot M(\xi^+_{j-\frac{1}{2}} - \xi^-_{j-\frac{1}{2}}) = \left(\widehat{K\xi}\right)_{j-\frac{1}{2}} \cdot M(\xi^+_{j-\frac{1}{2}} - \xi^-_{j-\frac{1}{2}}), \end{aligned}$$

which leads to the conclusion that $\Theta_{j-\frac{1}{2}} = 0$.

For the right-hand side of (4.6), we have

$$-B_j(\eta, M\xi) = -\int_{I_j} M\eta_t \cdot M\xi dx + \int_{I_j} K\eta \cdot M(\xi)_x dx - \left(\widehat{K\eta} \cdot M\xi^-\right)_{j+\frac{1}{2}} + \left(\widehat{K\eta} \cdot M\xi^+\right)_{j-\frac{1}{2}},$$

in which the second term on the right-hand side vanishes and $\widehat{K\eta} = 0$ according to the definition of the projection P. It follows that

$$-B_j(\eta, M\xi) = -\int_{I_j} M\eta_t \cdot M\xi dx \leqslant \frac{1}{2}\left(\|M\eta_t\|_j^2 + \|M\xi\|_j^2\right). \tag{4.7}$$

Since $\boldsymbol{z}$ is assumed to be bounded, $\boldsymbol{z}_h$ is also bounded following (4.5). With the definition of S in (2.7), there exists some $L > 0$ such that

$$\|(\nabla_{\boldsymbol{z}} S)(\boldsymbol{z}) - (\nabla_{\boldsymbol{z}} S)(\boldsymbol{z}_h)\|_j \leqslant L\|\boldsymbol{z} - \boldsymbol{z}_h\|_j,$$

and therefore

$$\begin{aligned}\int_{I_j} [(\nabla_{\boldsymbol{z}} S)(\boldsymbol{z}) - (\nabla_{\boldsymbol{z}} S)(\boldsymbol{z}_h)] \cdot M\xi dx \leqslant & L\left(\|\eta + \xi\|_j^2 + \|M\xi\|_j^2\right) \\ \leqslant & 2L\left(\|\eta\|_j^2 + \|\xi\|_j^2 + \|M\xi\|_j^2\right).\end{aligned} \tag{4.8}$$

Plugging these into the equation (4.6) and summing up over j, we get

$$\begin{aligned}\frac{d}{dt}\|M\xi\|^2 \leqslant & \|M\eta_t\|^2 + \|M\xi\|^2 + 4L\left(\|\eta\|^2 + \|\xi\|^2 + \|M\xi\|^2\right) \\ = & (1+4L)\|M\xi\|^2 + \|M\eta_t\|^2 + 4L\|\eta\|^2 + 4L\|\xi\|^2 \\ \leqslant & (1+4L)\|M\xi\|^2 + 4L\|\xi\|^2 + Ch^{2k+2},\end{aligned}$$

in which the last inequality comes from the projection error (4.2). Note that for the NLD equation, $\|M\boldsymbol{z}_h\| = \|\boldsymbol{z}_h\|$ with the choice of M in (2.6). Therefore, we have

$$\frac{d}{dt}\|\xi\|^2 \leqslant (1+8L)\|\xi\|^2 + Ch^{2k+2}.$$

Applying the Grönwall's inequality, the optimal initial error, and the projection error (4.2) give us the optimal error estimate

$$\|\boldsymbol{z} - \boldsymbol{z}_h\| \leqslant Ch^{k+1},$$

as desired.

To complete the proof, let us verify the a priori assumption (4.4). Easy to observe that it holds at time $t = 0$, because $\|\boldsymbol{z}(x,0) - \boldsymbol{z}_h(x,0)\| = O(h^{k+1})$. Let us define

$$t^* = \inf\{t : \ \|\boldsymbol{z} - \boldsymbol{z}_h\| > h\}.$$

If $t^* < T$, then at $t = t^*$, we have $\|\boldsymbol{z} - \boldsymbol{z}_h\| = h$ by continuity. On the other hand, we have $\|\boldsymbol{z} - \boldsymbol{z}_h\| \leqslant Ch^{k+1}$ at $t = t^*$, therefore, we have $h \leqslant Ch^{k+1}$, which is a contradiction if $k \geqslant 1$ and h is sufficiently small. Therefore, we have $t^* \geq T$ and this justifies our a priori assumption (4.4), which finishes the proof. □

Remark 4.1. One fact about the NLD equation is that $\|M\boldsymbol{z}_h\| = \|\boldsymbol{z}_h\|$, which is utilized in the proof. This condition can be relaxed to the invertibility of the matrix M. Note that this proof of optimal error estimate may not work for the general HPDE studied in [48], especially in the case when the matrix M in the HPDE system is singular, including the Korteweg-de Vries equation, and Camassa-Holm equation, etc.

5. High order energy conserving SAV temporal discretization

In this section, we apply high order energy conserving SAV method to the semi-discrete DG discretization (3.1) of the NLD equation. The second order method will be discussed first, followed by extension to higher order methods.

Following the SAV approach [46], we extract the quadratic terms

$$S_1(\boldsymbol{z}) = -\frac{1}{2}m(p_1^2 + q_1^2 - p_2^2 - q_2^2),$$

from the function S and introduce the auxiliary function

$$r(t) = \sqrt{\int_\Omega S_2(\boldsymbol{z}(x,t))dx},$$

where $S_2(\boldsymbol{z}) = \frac{1}{2}\lambda(p_1^2 + q_1^2 - p_2^2 - q_2^2)^2$ is always nonnegative. Now we can rewrite the NLD equation (2.5) as

$$\begin{cases} M\boldsymbol{z}_t + K\boldsymbol{z}_x = \nabla_{\boldsymbol{z}} S_1(\boldsymbol{z}) + r(t) b(\boldsymbol{z}(x,t)), \\ \dfrac{d}{dt} r(t) = \dfrac{1}{2} \displaystyle\int_\Omega b(\boldsymbol{z}(x,t)) \cdot \boldsymbol{z}_t dx, \\ r(0) = \sqrt{\displaystyle\int_\Omega S_2(\boldsymbol{z}(x,0)) dx}, \end{cases} \tag{5.1}$$

where $b(\boldsymbol{z}(x,t)) = \frac{\nabla_{\boldsymbol{z}} S_2(\boldsymbol{z})}{\sqrt{\int S_2(\boldsymbol{z}(x,t))dx}}$. Note that this reformulation replaces part of the function S with a new term involving the new variable $r(t)$. The first order spatial derivatives are not affected, and after applying the semi-discrete DG spatial discretization, it can be shown that the optimal semi-discrete error estimate, charge conservation, energy conservation properties in the previous section still hold for the new system.

5.1. Second order SAV method

For simplicity we introduce the following notations:

$$D_t u^n = \frac{u^{n+1} - u^n}{\Delta t}, \quad u^{n+\frac{1}{2}} = \frac{1}{2}(u^n + u^{n+1}), \quad u^{n*} = \frac{3}{2}u^n - \frac{1}{2}u^{n-1},$$

$$(u,v)_j = \int_{I_j} v^T u dx, \quad (u,v) = \int_\Omega v^T u dx, \quad \widehat{K\boldsymbol{z}^n} \cdot \boldsymbol{\phi}\Big|_{j-\frac{1}{2}}^{j+\frac{1}{2}} = \left(\widehat{K\boldsymbol{z}^n} \cdot \boldsymbol{\phi}^-\right)_{j+\frac{1}{2}} - \left(\widehat{K\boldsymbol{z}^n} \cdot \boldsymbol{\phi}^+\right)_{j-\frac{1}{2}}.$$

Following the approach in [33,46], we can obtain the second order fully discrete SAV-DG scheme

$$(MD_t\boldsymbol{z}_h^n, \boldsymbol{\phi})_j = (K\boldsymbol{z}_h^{n+\frac{1}{2}}, \boldsymbol{\phi}_x)_j - \widehat{K\boldsymbol{z}_h^{n+\frac{1}{2}}} \cdot \boldsymbol{\phi}\Big|_{j-\frac{1}{2}}^{j+\frac{1}{2}} + (\nabla_{\boldsymbol{z}} S_1(\boldsymbol{z}_h^{n+\frac{1}{2}}), \boldsymbol{\phi})_j + r^{n+\frac{1}{2}}(b(\boldsymbol{z}_h^{n*}), \boldsymbol{\phi})_j, \tag{5.2a}$$

$$D_t r^n = \frac{1}{2}(b(\boldsymbol{z}_h^{n*}), D_t\boldsymbol{z}_h^n), \tag{5.2b}$$

with the numerical fluxes $\widehat{K\boldsymbol{z}_h}$ defined in (3.2). At first glance, this scheme appears to be an implicit coupled method. However, as illustrated below, we are able to eliminate $r^{n+\frac{1}{2}}$ and deduce a simple formula to evaluate r^{n+1} and $\boldsymbol{z}_h^{n+1}$, which involves only one matrix inversion that could be pre-calculated and re-used at each time step.

Easy to observe that $\nabla_{\boldsymbol{z}} S_1(\boldsymbol{z}) = D\boldsymbol{z}$, where $D = \mathrm{diag}(-m, -m, m, m)$. We can rewrite the scheme (5.2) as

$$\begin{aligned} \frac{1}{\Delta t}(M(\boldsymbol{z}_h^{n+1} - \boldsymbol{z}_h^n), \boldsymbol{\phi})_j = {} & \frac{1}{2}(K(\boldsymbol{z}_h^n + \boldsymbol{z}_h^{n+1}), \boldsymbol{\phi}_x)_j - \frac{1}{2}\widehat{K\boldsymbol{z}_h^n} \cdot \boldsymbol{\phi}\Big|_{j-\frac{1}{2}}^{j+\frac{1}{2}} - \frac{1}{2}\widehat{K\boldsymbol{z}_h^{n+1}} \cdot \boldsymbol{\phi}\Big|_{j-\frac{1}{2}}^{j+\frac{1}{2}} \\ & + \frac{1}{2}(D(\boldsymbol{z}_h^n + \boldsymbol{z}_h^{n+1}), \boldsymbol{\phi})_j + \frac{1}{2}(r^n + r^{n+1})(b(\boldsymbol{z}_h^{n*}), \boldsymbol{\phi})_j, \\ r^{n+1} - r^n = {} & \frac{1}{2}(b(\boldsymbol{z}_h^{n*}), \boldsymbol{z}_h^{n+1} - \boldsymbol{z}_h^n), \end{aligned}$$

which can be rearranged as

$$\begin{aligned} & \left(\frac{1}{\Delta t}M\boldsymbol{z}_h^{n+1} - \frac{1}{2}D\boldsymbol{z}_h^{n+1}, \boldsymbol{\phi}\right)_j - \frac{1}{2}(K\boldsymbol{z}_h^{n+1}, \boldsymbol{\phi}_x)_j + \frac{1}{2}\widehat{K\boldsymbol{z}_h^{n+1}} \cdot \boldsymbol{\phi}\Big|_{j-\frac{1}{2}}^{j+\frac{1}{2}} \\ & \quad = \left(\frac{1}{\Delta t}M\boldsymbol{z}_h^n + \frac{1}{2}D\boldsymbol{z}_h^n + \frac{r^n + r^{n+1}}{2}b(\boldsymbol{z}_h^{n*}), \boldsymbol{\phi}\right)_j + \frac{1}{2}(K\boldsymbol{z}_h^n, \boldsymbol{\phi}_x)_j - \frac{1}{2}\widehat{K\boldsymbol{z}_h^n} \cdot \boldsymbol{\phi}\Big|_{j-\frac{1}{2}}^{j+\frac{1}{2}}, \end{aligned} \tag{5.3a}$$

$$r^{n+1} = r^n - \frac{1}{2}(b(\boldsymbol{z}_h^{n*}), \boldsymbol{z}_h^n) + \frac{1}{2}(b(\boldsymbol{z}_h^{n*}), \boldsymbol{z}_h^{n+1}). \tag{5.3b}$$

Let us define the linear operator $\mathcal{L}: \boldsymbol{V}_h \to \boldsymbol{V}_h$ as

$$(\mathcal{L}\boldsymbol{z}_h^n, \boldsymbol{\phi}) = (K\boldsymbol{z}_h^n, \boldsymbol{\phi}_x) - \sum_j \widehat{K(\boldsymbol{z}_h^n)_j} \cdot \boldsymbol{\phi}\Big|_{j-\frac{1}{2}}^{j+\frac{1}{2}}, \quad \forall \boldsymbol{\phi} \in \boldsymbol{V}_h,$$

and represent it by the matrix L. We can then define the block diagonal matrix $P_\pm = \mathrm{diag}(\frac{1}{\Delta t}M \pm \frac{1}{2}D, \cdots, \frac{1}{\Delta t}M \pm \frac{1}{2}D)$ with the dimension $4(k+1)N \times 4(k+1)N$, where k is the polynomial degree of DG method and N is the number of cells. We take the sum of (5.3a) over j and get

$$((P_- - L/2)\boldsymbol{z}_h^{n+1}, \boldsymbol{\phi}) = ((P_+ + L/2)\boldsymbol{z}_h^n, \boldsymbol{\phi}) + \frac{r^n + r^{n+1}}{2}(b(\boldsymbol{z}_h^{n*}), \boldsymbol{\phi}).$$

As this holds for all $\boldsymbol{\phi} \in \boldsymbol{V}_h$, it follows that

$$(P_- - L/2)\boldsymbol{z}_h^{n+1} = (P_+ + L/2)\boldsymbol{z}_h^n + \frac{r^n + r^{n+1}}{2}\Pi b(\boldsymbol{z}_h^{n*}),$$

where $\Pi b(\boldsymbol{z}_h^{n*})$ stands for the piecewise L^2 projection of $b(\boldsymbol{z}_h^{n*})$ onto $\boldsymbol{V}_h$. Replacing r^{n+1} by the formula in (5.3b) yields

$$(P_- - L/2)\boldsymbol{z}_h^{n+1} = (P_+ + L/2)\boldsymbol{z}_h^n + \left(r^n - \frac{1}{4}(b(\boldsymbol{z}_h^{n*}), \boldsymbol{z}_h^n) + \frac{1}{4}(b(\boldsymbol{z}_h^{n*}), \boldsymbol{z}_h^{n+1})\right)\Pi b(\boldsymbol{z}_h^{n*}).$$

Let $Q_\pm = P_\pm \pm L/2$ and

$$\xi^n = Q_+\boldsymbol{z}_h^n + \left(r^n - \frac{1}{4}(b(\boldsymbol{z}_h^{n*}), \boldsymbol{z}_h^n)\right)\Pi b(\boldsymbol{z}_h^{n*}), \tag{5.4}$$

which leads to

$$\boldsymbol{z}_h^{n+1} = Q_-^{-1}\xi^n + \frac{1}{4}(b(\boldsymbol{z}_h^{n*}), \boldsymbol{z}_h^{n+1})Q_-^{-1}\Pi b(\boldsymbol{z}_h^{n*}). \tag{5.5}$$

Taking the inner product of (5.5) with $b(\boldsymbol{z}_h^{n*})$ gives us

$$(b(\boldsymbol{z}_h^{n*}), \boldsymbol{z}_h^{n+1}) = (b(\boldsymbol{z}_h^{n*}), Q_-^{-1}\xi^n) + \frac{1}{4}(b(\boldsymbol{z}_h^{n*}), \boldsymbol{z}_h^{n+1})(b(\boldsymbol{z}_h^{n*}), Q_-^{-1}\Pi b(\boldsymbol{z}_h^{n*})),$$

and therefore

$$(b(\boldsymbol{z}_h^{n*}), \boldsymbol{z}_h^{n+1}) = \frac{(b(\boldsymbol{z}_h^{n*}), Q_-^{-1}\xi^n)}{1 - \frac{1}{4}(b(\boldsymbol{z}_h^{n*}), Q_-^{-1}\Pi b(\boldsymbol{z}_h^{n*}))}.$$

Inserting this into (5.3b) and (5.5), we finally obtain the efficient way to implement the SAV-DG method (5.2) as:

$$r^{n+1} = r^n - \frac{1}{2}(b(\boldsymbol{z}_h^{n*}), \boldsymbol{z}_h^n) + \frac{2(b(\boldsymbol{z}_h^{n*}), Q_-^{-1}\xi^n)}{4 - (b(\boldsymbol{z}_h^{n*}), Q_-^{-1}\Pi b(\boldsymbol{z}_h^{n*}))}, \tag{5.6a}$$

$$\boldsymbol{z}_h^{n+1} = Q_-^{-1}\xi^n + \frac{(b(\boldsymbol{z}_h^{n*}), Q_-^{-1}\xi^n)}{4 - (b(\boldsymbol{z}_h^{n*}), Q_-^{-1}\Pi b(\boldsymbol{z}_h^{n*}))}Q_-^{-1}\Pi b(\boldsymbol{z}_h^{n*}). \tag{5.6b}$$

Next, we will explore the energy-conserving property of the scheme (5.2). Recall that the energy density is defined by $\rho_E(\boldsymbol{z}) = S_1(\boldsymbol{z}) + S_2(\boldsymbol{z}) - \frac{1}{2}K\boldsymbol{z}_x \cdot \boldsymbol{z}$, and the semi-discrete DG method conserves the energy of the form (3.8) in Proposition 3.2. We have the following theorem on the conservation of a slightly modified energy of the fully discrete method.

Theorem 5.1. *The numerical solution $\boldsymbol{z}_h$ of the SAV-DG scheme (5.2) with periodic boundary condition conserves the discrete total energy*

$$\mathcal{E}^n = \int \left(S_1^n - \frac{1}{2}K(\boldsymbol{z}_h^n)_x \cdot \boldsymbol{z}_h^n\right)dx + (r^n)^2 + \frac{1}{2}\sum_j \left((K\{\boldsymbol{z}_h^n\} + A[\boldsymbol{z}_h^n]) \cdot [\boldsymbol{z}_h^n]\right)_{j+\frac{1}{2}}. \tag{5.7}$$

Proof. By taking the test function $\boldsymbol{\phi} = D_t\boldsymbol{z}_h^n$ in (5.2a), we observe that the first term disappears due to the skew-symmetric matrix M, and this leads to

$$(\nabla_{\boldsymbol{z}}S_1(\boldsymbol{z}_h^{n+\frac{1}{2}}), D_t\boldsymbol{z}_h^n)_j + r^{n+\frac{1}{2}}(b(\boldsymbol{z}_h^{n*}), D_t\boldsymbol{z}_h^n)_j = (KD_t(\boldsymbol{z}_h^n)_x, \boldsymbol{z}_h^{n+\frac{1}{2}})_j + \widehat{K\boldsymbol{z}_h^{n+\frac{1}{2}}} \cdot D_t\boldsymbol{z}_h^n\Big|_{j-\frac{1}{2}}^{j+\frac{1}{2}}.$$

Since S_1 is the quadratic component of the function S, we have $D_t\int_{I_j} S_1^n dx = (\nabla_{\boldsymbol{z}}S_1(\boldsymbol{z}_h^{n+\frac{1}{2}}), D_t\boldsymbol{z}_h^n)_j$, therefore, we have

$$D_t\left(\int_{I_j} S_1^n dx + (r^n)^2\right) = (\nabla_{\boldsymbol{z}} S_1(\boldsymbol{z}_h^{n+\frac{1}{2}}), D_t\boldsymbol{z}_h^n)_j + r^{n+\frac{1}{2}}(b(\boldsymbol{z}_h^{n*}), D_t\boldsymbol{z}_h^n)_j$$

$$= (KD_t(\boldsymbol{z}_h^n)_x, \boldsymbol{z}_h^{n+\frac{1}{2}})_j + \widehat{K\boldsymbol{z}_h^{n+\frac{1}{2}}} \cdot D_t\boldsymbol{z}_h^n\Big|_{j-\frac{1}{2}}^{j+\frac{1}{2}}.$$

By repeatedly using the fact that $D_t(a^n \cdot b^n) = D_t(a^n) \cdot b^{n+\frac{1}{2}} + a^{n+\frac{1}{2}} \cdot D_t(b^n)$, we have

$$\begin{aligned}
&D_t\left(\int_{I_j}\left(S_1^n - \frac{1}{2}K(\boldsymbol{z}_h^n)_x \cdot \boldsymbol{z}_h^n\right)dx + (r^n)^2 - \frac{1}{2}\widehat{K\boldsymbol{z}_h^n} \cdot \boldsymbol{z}_h^n\Big|_{j-\frac{1}{2}}^{j+\frac{1}{2}}\right)\\
=&(KD_t(\boldsymbol{z}_h^n)_x, \boldsymbol{z}_h^{n+\frac{1}{2}})_j + \widehat{K\boldsymbol{z}_h^{n+\frac{1}{2}}} \cdot D_t\boldsymbol{z}_h^n\Big|_{j-\frac{1}{2}}^{j+\frac{1}{2}} - \frac{1}{2}(KD_t(\boldsymbol{z}_h^n)_x, \boldsymbol{z}_h^{n+\frac{1}{2}})_j - \frac{1}{2}(K(\boldsymbol{z}_h^{n+\frac{1}{2}})_x, D_t\boldsymbol{z}_h^n)_j\\
&-\frac{1}{2}\left(\widehat{K\boldsymbol{z}_h^{n+\frac{1}{2}}} \cdot D_t\boldsymbol{z}_h^n + \widehat{KD_t\boldsymbol{z}_h^n} \cdot \boldsymbol{z}_h^{n+\frac{1}{2}}\right)\Big|_{j-\frac{1}{2}}^{j+\frac{1}{2}}\\
=&\frac{1}{2}(KD_t(\boldsymbol{z}_h^n)_x, \boldsymbol{z}_h^{n+\frac{1}{2}})_j - \frac{1}{2}(K(\boldsymbol{z}_h^{n+\frac{1}{2}})_x, D_t\boldsymbol{z}_h^n)_j + \frac{1}{2}\left(\widehat{K\boldsymbol{z}_h^{n+\frac{1}{2}}} \cdot D_t\boldsymbol{z}_h^n - \widehat{KD_t\boldsymbol{z}_h^n} \cdot \boldsymbol{z}_h^{n+\frac{1}{2}}\right)\Big|_{j-\frac{1}{2}}^{j+\frac{1}{2}}\\
=&-\frac{1}{2}\int_{I_j}(K\boldsymbol{z}_h^{n+\frac{1}{2}} \cdot D_t\boldsymbol{z}_h^n)_x dx + \frac{1}{2}\left(\widehat{K\boldsymbol{z}_h^{n+\frac{1}{2}}} \cdot D_t\boldsymbol{z}_h^n - \widehat{KD_t\boldsymbol{z}_h^n} \cdot \boldsymbol{z}_h^{n+\frac{1}{2}}\right)\Big|_{j-\frac{1}{2}}^{j+\frac{1}{2}}\\
=&-\frac{1}{2}\left(K\boldsymbol{z}_h^{n+\frac{1}{2}} \cdot D_t\boldsymbol{z}_h^n - \widehat{K\boldsymbol{z}_h^{n+\frac{1}{2}}} \cdot D_t\boldsymbol{z}_h^n + \widehat{KD_t\boldsymbol{z}_h^n} \cdot \boldsymbol{z}_h^{n+\frac{1}{2}}\right)\Big|_{j-\frac{1}{2}}^{j+\frac{1}{2}}\\
=:&-F(\boldsymbol{z}_h^{n+\frac{1}{2}}, D_t\boldsymbol{z}_h^n)\Big|_{j-\frac{1}{2}}^{j+\frac{1}{2}},
\end{aligned}$$

where $F(\boldsymbol{z}_1, \boldsymbol{z}_2) := \frac{1}{2}\left(K\boldsymbol{z}_1 \cdot \boldsymbol{z}_2 - \widehat{K\boldsymbol{z}_1} \cdot \boldsymbol{z}_2 + \widehat{K\boldsymbol{z}_2} \cdot \boldsymbol{z}_1\right)$. Using the fact that A is symmetric and K is skew-symmetric, we have

$$\begin{aligned}
&2F(\boldsymbol{z}_1, \boldsymbol{z}_2)(x^+_{j+\frac{1}{2}}) - 2F(\boldsymbol{z}_1, \boldsymbol{z}_2)(x^-_{j+\frac{1}{2}})\\
=&K\boldsymbol{z}_1^+ \cdot \boldsymbol{z}_2^+ - K\boldsymbol{z}_1^- \cdot \boldsymbol{z}_2^- - (K\{\boldsymbol{z}_1\} + A[\boldsymbol{z}_1]) \cdot [\boldsymbol{z}_2] + (K\{\boldsymbol{z}_2\} + A[\boldsymbol{z}_2]) \cdot [\boldsymbol{z}_1]\\
=&K\boldsymbol{z}_1^+ \cdot \boldsymbol{z}_2^+ - K\boldsymbol{z}_1^- \cdot \boldsymbol{z}_2^- - \frac{1}{2}K(\boldsymbol{z}_1^+ + \boldsymbol{z}_1^-) \cdot (\boldsymbol{z}_2^+ - \boldsymbol{z}_2^-) + \frac{1}{2}K(\boldsymbol{z}_2^+ + \boldsymbol{z}_2^-) \cdot (\boldsymbol{z}_1^+ - \boldsymbol{z}_1^-) = 0,
\end{aligned}$$

at any cell interface $x_{j+\frac{1}{2}}$. Finally, we can sum over all the cells I_j and obtain

$$D_t(\mathcal{E}^n) = D_t\left(\int_\Omega\left(S_1^n - \frac{1}{2}K(\boldsymbol{z}_h^n)_x \cdot \boldsymbol{z}_h^n\right)dx + (r^n)^2 + \frac{1}{2}\sum_j\left((K\{\boldsymbol{z}_h^n\} + A[\boldsymbol{z}_h^n]) \cdot [\boldsymbol{z}_h^n]\right)_{j+\frac{1}{2}}\right) = 0,$$

which finishes the proof of the conservation of the discrete total energy $\mathcal{E}^n$ defined in (5.7). □

As explained in Remark 3.1, the boundary terms in the definition of the discrete total energy $\mathcal{E}^n$ in (5.7) can be absorbed into the numerical derivative operator for specific matrix A. One difference between the discrete total energy $\mathcal{E}^n$ in (5.7) and the original energy lies in the term $(r^n)^2$, which approximates $\int_\Omega S_2(\boldsymbol{z}(x,t))dx$, therefore, the energy $\mathcal{E}^n$ in (5.7) can be viewed as an approximation of the original energy of the system.

Remark 5.1. It can be shown that the fully implicit midpoint temporal discretization combined with the semi-discrete DG scheme (3.1) achieves the charge conservation at the discrete level. However, the computational cost of such a fully implicit method is higher than that of the proposed SAV method and we do not pursue it here.

5.2. Higher order SAV method

As the DG spatial discretization can yield high order spatial accuracy, we explore the high order SAV time discretization in this section. One approach is to utilize the fourth order Gauss-Legendre Runge-Kutta method [4] to formulate the high order version of the SAV-DG scheme in (5.2). We can prove the conservation of the same energy as in Theorem 5.1. However, the implementation of this method is more complicated than that of the second order case. Below, we use a different approach to achieve fourth order temporal accuracy by reusing the second order method (5.2) and iterating it three times.

In the second order SAV-DG method (5.2), we can rewrite the equation (5.2a) as

$$\boldsymbol{z}_h^{n+1} = \boldsymbol{z}_h^n + \Delta t \left[f\left(\frac{1}{2}(\boldsymbol{z}_h^n + \boldsymbol{z}_h^{n+1})\right) + \frac{1}{2}(r^n + r^{n+1}) g(\boldsymbol{z}_h^{n*}) \right],$$

with some linear function f and some (nonlinear) function g. As shown in [40], one can obtain a fourth order accurate method by iterating this solver in the following way

$$\begin{aligned}
\boldsymbol{z}_1 &= \boldsymbol{z}_h^n + b_1 \Delta t \left[f\left(\frac{1}{2}(\boldsymbol{z}_h^n + \boldsymbol{z}_1)\right) + \frac{1}{2}(r^n + r_1) g(\boldsymbol{z}_1^*) \right], \\
\boldsymbol{z}_2 &= \boldsymbol{z}_1 + b_2 \Delta t \left[f\left(\frac{1}{2}(\boldsymbol{z}_1 + \boldsymbol{z}_2)\right) + \frac{1}{2}(r_1 + r_2) g(\boldsymbol{z}_2^*) \right], \\
\boldsymbol{z}_h^{n+1} &= \boldsymbol{z}_2 + b_3 \Delta t \left[f\left(\frac{1}{2}(\boldsymbol{z}_2 + \boldsymbol{z}_h^{n+1})\right) + \frac{1}{2}(r_2 + r^{n+1}) g(\boldsymbol{z}_3^*) \right],
\end{aligned} \tag{5.8}$$

with properly chosen coefficients

$$b_1 = b_3 = \frac{1}{2 - 2^{1/3}}, \qquad b_2 = 1 - 2b_3,$$

and

$$\boldsymbol{z}_1^* \approx \boldsymbol{z}\left(t^n + \frac{1}{2} b_1 \Delta t\right), \qquad \boldsymbol{z}_2^* \approx \boldsymbol{z}\left(t^n + (b_1 + \frac{1}{2} b_2)\Delta t\right), \qquad \boldsymbol{z}_3^* \approx \boldsymbol{z}\left(t^n + (b_1 + b_2 + \frac{1}{2} b_3)\Delta t\right).$$

If we approximate them by $\boldsymbol{z}_1^* = \frac{1}{2}(\boldsymbol{z}^n + \boldsymbol{z}_1)$, $\boldsymbol{z}_2^* = \frac{1}{2}(\boldsymbol{z}_1 + \boldsymbol{z}_2)$, $\boldsymbol{z}_3^* = \frac{1}{2}(\boldsymbol{z}_2 + \boldsymbol{z}^{n+1})$, the method (5.8) is exactly the fourth order Runge-Kutta method with the Butcher tableau given by

$b_1/2$	$b_1/2$			
$b_1 + b_2/2$	b_1	$b_2/2$		
$b_1 + b_2 + b_3/2$	b_1	b_2	$b_3/2$	
	b_1	b_2	b_3	

However, this may be difficult to solve directly as g is a nonlinear function. Instead, we follow the similar idea as in the second order case, and seek to approximate these $\boldsymbol{z}_i^*$ by the values of $\boldsymbol{z}$ at previous time steps with sufficient accuracy.

In order to maintain the 4th order of accuracy, we consider the values $\boldsymbol{z}^{n-j}$ with $j = 0, 1, 2, 3$ at the current and previous time steps. One can use interpolation to obtain an approximation of $\boldsymbol{z}_i^*$:

$$\begin{pmatrix} \boldsymbol{z}_1^* \\ \boldsymbol{z}_2^* \\ \boldsymbol{z}_3^* \end{pmatrix} = \begin{pmatrix} 2.746442253737104 & 2.1875 & 1.705649303565513 \\ -3.322097661811303 & -2.1875 & -1.253340387175503 \\ 2.080472158391121 & 1.3125 & 0.714129267674637 \\ -0.504816750316923 & -1.3125 & -0.166438184064648 \end{pmatrix}^T \begin{pmatrix} \boldsymbol{z}^n \\ \boldsymbol{z}^{n-1} \\ \boldsymbol{z}^{n-2} \\ \boldsymbol{z}^{n-3} \end{pmatrix}.$$

Correspondingly, the other equation (5.2b) can be modified into three stages in the same way:

$$\begin{aligned}
r_1 - r^n &= \frac{1}{2}(b(\boldsymbol{z}_1^*), \boldsymbol{z}_1 - \boldsymbol{z}_h^n), \\
r_2 - r_1 &= \frac{1}{2}(b(\boldsymbol{z}_2^*), \boldsymbol{z}_2 - \boldsymbol{z}_1), \\
r^{n+1} - r_2 &= \frac{1}{2}(b(\boldsymbol{z}_3^*), \boldsymbol{z}_h^{n+1} - \boldsymbol{z}_2).
\end{aligned} \tag{5.9}$$

When evaluating the solutions $\boldsymbol{z}_h^{n+1}$, r^{n+1} $(n \geqslant 3)$, at the next time step, we first use $\boldsymbol{z}_h^{n-j}(j = 0, 1, 2, 3)$ to compute the variables $\boldsymbol{z}_i^*$. Then following the similar derivation to derive the efficient formulae (5.6), one can evaluate the intermediate values $r_1, \boldsymbol{z}_1$, $r_2, \boldsymbol{z}_2$, and eventually the numerical solutions r^{n+1} and $\boldsymbol{z}_h^{n+1}$. Since more than one initial condition $\boldsymbol{z}_h^0$ is needed, in practical implementation, we can use a fourth-order numerical method to solve for $\boldsymbol{z}_h^1$ and $\boldsymbol{z}_h^2$, and the above scheme can be applied from the third time step.

Table 1
Spatial accuracy test of the SAV-DG method when $k = 1$ in Section 6.1.

N	$v = 0$		$v = -0.2$	
	L^2 error	Order	L^2 error	Order
100	9.162e-03		1.070e-02	
200	2.420e-03	1.920	2.909e-03	1.879
400	5.850e-04	2.049	6.947e-04	2.066
800	1.472e-04	1.991	1.766e-04	1.976

Table 2
Spatial accuracy test of the SAV-DG method when $k = 2$ in Section 6.1.

N	$v = 0$		$v = -0.2$	
	L^2 error	Order	L^2 error	Order
100	3.913e-04		5.245e-04	
200	4.988e-05	2.972	6.362e-05	3.043
400	6.517e-06	2.936	8.559e-06	2.894
800	8.378e-07	2.960	1.079e-06	2.987

Remark 5.2. Since each stage in the higher order scheme is of the same pattern as (5.2), we can claim that the discrete energy (5.7) is conserved in every intermediate stage. The proof is identical to that of Theorem 5.1 and will be ignored here. Hence the DG discretization combined with the higher order SAV time integration still conserves the discrete energy (5.7).

6. Numerical examples

In this section, some numerical results are provided to demonstrate the behavior of the proposed energy conserving SAV-DG methods for the NLD equation. In our simulations, we set $m = 1$ and $\lambda = \frac{1}{2}$ in (2.7), and adopt the periodic boundary condition or non-reflecting boundary condition. We consider the DG method with various polynomial degree k as the spatial discretization, and the second or fourth order SAV method for temporal discretization. The projection P defined in Lemma 4.1 is utilized to set $\boldsymbol{z}_h^0 = P\boldsymbol{z}(x, 0)$ as the initial condition. The alternating numerical flux is chosen in the numerical examples.

6.1. Accuracy test

Some exact solutions are discussed in Remark 2.1, which will be used to test the order of accuracy of our schemes. We consider two cases: $v = 0$ (standing wave) and $v = -0.2$ (a solitary wave traveling from right to left). The other parameters are set as $x_0 = 5$ and $\Lambda = 0.8$, and the computational domain is taken to be $[-35, 35]$.

We first test the convergence rate of the DG spatial discretization, by employing a very small time step size $\Delta t = 0.001$ so that the error will be dominated by the spatial discretization. The stopping time is set as $T = 1$. When the linear polynomials ($k = 1$) or quadratic polynomials ($k = 2$) are used in the DG discretization, the convergence rate is expected to be 2 or 3, as indicated by Theorem 4.2 for the semi-discrete methods. The L^2 errors and numerical orders of our SAV-DG methods (5.2) with various grids N and different finite element bases are shown in Table 1 and Table 2, respectively. The numerical order is computed by $\log_{N_i/N_{i+1}}(e_{i+1}/e_i)$ where N_i and e_i represent the number of elements and the L^2 error respectively. From the tables, we can observe the second order and the third order convergence as desired, which indicates the optimal order of the DG spatial discretization.

Next, we validate the temporal accuracy of the second order SAV-DG method (5.2) and the high order SAV-DG method (5.8)-(5.9). We fix N to be 800 and choose the quadratic polynomials ($k = 2$) as the finite element basis. This time we choose relatively large Δt so that the temporal discretization dominates the error of the scheme and the convergence rate of the temporal discretization can be observed. In this test, since the exact solution is available, we set $\boldsymbol{z}_h^{-i} = P\boldsymbol{z}(x, -i\Delta t)$ ($i = 1, 2, 3$) for the high order SAV-DG method, so that the approximation at the first few time steps is consistent with the others and of the same order. For the second order SAV-DG method (5.2), the stopping time is chosen to be $T = 2$, and the L^2 errors and numerical orders of the numerical solutions with various time step sizes are shown in Table 3. From the table, we can easily observe the desired second order convergence rate as expected. For the fourth order SAV-DG method (5.8)-(5.9), the stopping time is chosen to be $T = 8$, and the L^2 errors and numerical orders of the numerical solutions with various time step sizes are shown in Table 4. Again, we can easily observe the high order convergence rate of this method, which is higher than 4. During the interpolation procedure to approximate z_i^*, we have tried to use only three values of z^{n-j} with $j = 0, 1, 2$ at the current and previous time steps, and the third order accuracy is observed numerically under that setup.

Table 3
Temporal accuracy test of the second order SAV-DG method in Section 6.1.

Δt	$v=0$		$v=-0.2$	
	L^2 error	Order	L^2 error	Order
0.2	1.052e-02		1.117e-02	
0.1	2.801e-03	1.909	2.977e-03	1.907
0.05	7.220e-04	1.956	7.677e-04	1.955
0.025	1.832e-04	1.978	1.949e-04	1.978
0.0125	4.615e-05	1.989	4.910e-05	1.989

Table 4
Temporal accuracy test of the high order SAV-DG method in Section 6.1.

	$v=0$		$v=-0.2$	
Δt	L^2 error	Order	L^2 error	Order
0.8	8.363e-01		1.021	
0.4	4.230e-02	4.305	5.356e-02	4.253
0.2	1.430e-03	4.887	1.891e-03	4.824
0.1	4.440e-05	5.009	6.436e-05	4.877
0.05	1.673e-06	4.730	2.785e-06	4.530

Table 5
The changes of discrete total energy at $T=50$ in Section 6.2.

Scheme	$v=0$	$v=-0.2$
$k=1$, 2nd order time integration	2.043e-14	2.909e-14
$k=2$, 2nd order time integration	6.684e-14	4.763e-14
$k=2$, 4th order time integration	3.997e-14	4.752e-14

6.2. Energy conservation

In Theorem 5.1, the conservation of the discrete energy defined in (5.7) was presented for the fully discrete SAV-DG methods. For the two examples studied in the previous section, we study their energy conservation property as well as their long time behavior. We set the number of the elements $N=140$ and $\Delta t=0.1$. The simulation is run for a long time until the final stopping time $T=50$. We implement both the second order SAV-DG method with the polynomial degree $k=1$ and $k=2$, and the fourth order SAV-DG method with $k=2$. We record the changes of discrete energy $\Delta\mathcal{E}=\mathcal{E}(T)-\mathcal{E}(0)$, and report the results of these methods at $T=50$ in Table 5. Fig. 1 shows how the discrete energy changes over time for the scheme using P^1 polynomials and 2nd order time integration. From them, we can observe that the changes are all around 10^{-14}, which indicates that they are at the level of the round-up error. This verifies the energy-conserving property of our method.

In [52], Xu et al. carried out a thorough review and numerical comparison of various numerical methods including the Crank-Nicolson (CN) schemes, the linearized CN schemes, Runge-Kutta DG (RKDG) methods, and the exponential operator splitting methods. The long time behavior of numerical error history of various methods can be found in [52, Fig. 1], from which one can observe that high order (energy dissipative) RKDG methods yield small numerical errors. Next we provide a comparison of performance between energy-preserving SAV-DG schemes and energy-dissipative SAV-DG or RKDG schemes. It is known that the DG method is energy-dissipative when upwind flux is used in the spatial discretization, as studied in [44]. For upwind flux, the matrix A in $\widetilde{K\boldsymbol{z}_h}=K\{\boldsymbol{z}_h\}+A[\boldsymbol{z}_h]$ takes the form

$$\begin{pmatrix} 0 & -\frac{1}{2} & 0 & 0 \\ \frac{1}{2} & 0 & 0 & 0 \\ 0 & 0 & 0 & -\frac{1}{2} \\ 0 & 0 & \frac{1}{2} & 0 \end{pmatrix},$$

which is not symmetric. We fix N to be 140 for P^1 polynomials. A small time step $\Delta t=0.005$ is used so that the numerical error is dominated by the spatial discretization. The simulation is run for the standing wave case ($v=0$). We also tried high order SAV method and P^2 polynomial basis with the choices of $N=70$ and $\Delta t=0.02$. In Fig. 2 the time history of L^2 errors is depicted for the SAV-DG schemes with different fluxes. The third order RKDG method is also included for comparison. We can observe that the L^2 errors of the schemes using upwind flux are much larger than those of the proposed schemes using alternating flux. This demonstrates that, with the same computational cost, the energy-preserving SAV-DG schemes are more accurate than the energy-dissipative DG methods in the long time simulation.

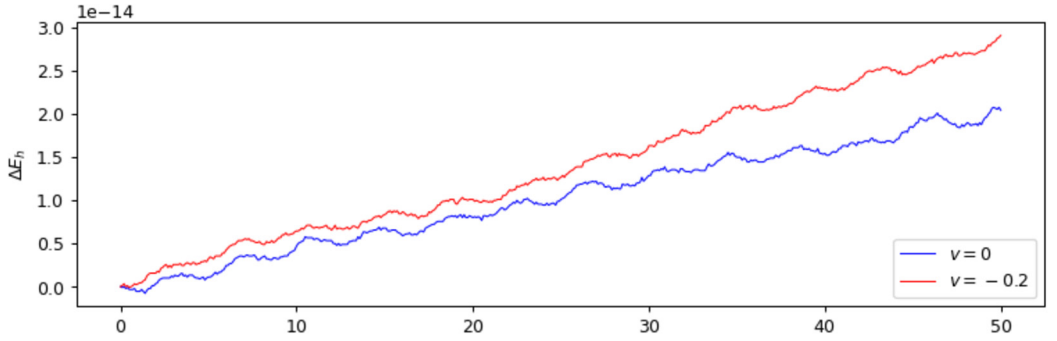

Fig. 1. The change of discrete total energy for the scheme using P^1 polynomials and 2nd order time integration in Section 6.2.

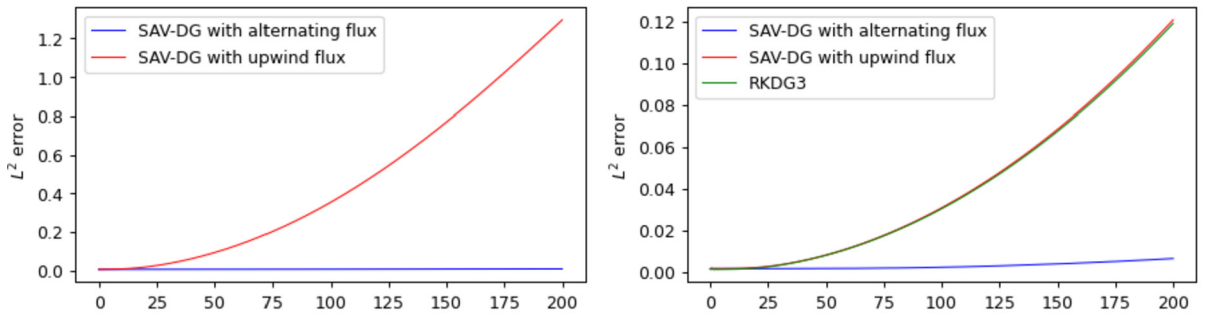

Fig. 2. The time history of L^2 errors for different methods in Section 6.2. Left: $k = 1$, $N = 140$, $\Delta t = 0.005$, 2nd order time integration; Right: $k = 2$, $N = 70$, $\Delta t = 0.02$, 4th order time integration.

6.3. Stability of standing waves

In [42], the stability of solitary waves in the NLD equation was investigated by Shao et al. via both theoretical and numerical approaches. A fourth-order operator splitting method was used to carry out the simulation. It was numerically observed that all stable nonlinear solitary waves have a one-hump profile (although not all one-hump waves are stable), and all two-hump waves are unstable. In this subsection, we will use the proposed SAV-DG scheme to validate the stability of standing waves with one hump and two humps. Analytically the standing wave does not change as time elapses. However, these steady states of charge may be stable or unstable for different frequencies Λ (which leads to either one- or two-hump profile).

The parameters in the standing wave solution (2.8) are chosen to be $x_0 = 0$ and $\Lambda = 0.5$ (one-hump) or 0.2 (two-hump). We take the number of grids N to be 800 and compute until $T = 70$ on the domain $[-50, 50]$. Fourth order SAV method with quadratic polynomials ($k = 2$) is used in the SAV-DG methods. We depict the change of discrete total energy and the time history of L^2 error in Fig. 3. For one-hump standing wave with $\Lambda = 0.5$, the numerical error accumulates very slowly. For two-hump standing wave with $\Lambda = 0.2$, the L^2 error starts to increase exponentially after some time. For instance, at $T = 40$, the L^2 error is less than 0.0003 and it increases to around 0.3 at $T = 70$. This is similar to the observation of the instability indicated in [42]. In spite of that, it can be seen that the changes of discrete total energy are conserved at the round-off error level in both cases, which is consistent with the energy conservation property outlined in Theorem 5.1.

6.4. Interaction of one-hump solitary waves

In this subsection we consider the interaction of two solitary waves solutions, with the initial conditions given by

$$\psi_1(x, 0) = \psi_{1l}^{ss}(x - x_l, 0) + \psi_{1r}^{ss}(x - x_r, 0), \tag{6.1a}$$

$$\psi_2(x, 0) = \psi_{2l}^{ss}(x - x_l, 0) + \psi_{2r}^{ss}(x - x_r, 0), \tag{6.1b}$$

where the solitary traveling wave solutions ψ_1^{ss}, ψ_2^{ss} are defined in (2.9a)-(2.9b). The parameters related to these two solitary waves are $x_l = -x_r = -8$; $\Lambda_l = 0.6$, $\Lambda_r = 0.8$; $v_l = \tanh(\theta_l)$ and $v_r = \tanh(\theta_r)$ with θ_l, θ_r given in Table 6. Here we consider three different cases as investigated in [1,44], with minor changes in the height and velocity of the initial waves.

The computational domain is taken as $[-50, 50]$. We choose $N = 500$ and run the simulation until $T = 150$ using quadratic polynomials ($k = 2$) as finite element basis with the fourth order time integration. In Fig. 4, we present the evolution of the charge density ρ_Q defined in (2.4) at various times. It can be observed that the initial shapes of three cases

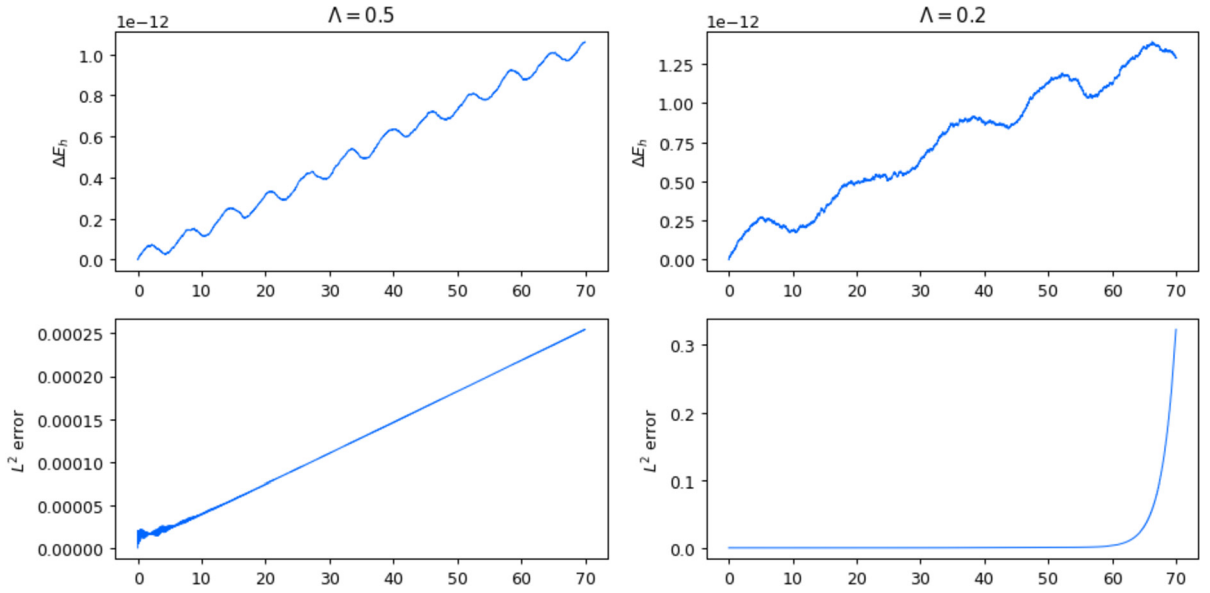

Fig. 3. The change of discrete total energy and the time history of L^2 error in Section 6.3.

Table 6
Three cases of the interaction dynamics for two solitary waves in Section 6.4.

Case	$T = 0$			
	θ_l	$-\theta_r$	Left wave crest	Right wave crest
(a)	0.150	0.237	0.807	0.410
(b)	0.183	0.288	0.811	0.415
(c)	0.200	0.314	0.814	0.418

Table 7
The propagation of two solitary waves in Section 6.4.

Case	Average velocity between $T = 90$ and 150		$T = 150$	
	$\overline{\theta_l}$	$-\overline{\theta_r}$	Left wave crest	Right wave crest
(a)	0.179	0.321	0.868 at $x = 19.7$	0.356 at $x = -39.7$
(b)	0.182	0.284	0.813 at $x = 21.3$	0.408 at $x = -37.3$
(c)	0.192	0.280	0.785 at $x = 22.9$	0.448 at $x = -37.5$

at $T = 0$ look similar, and the difference in the heights of these solitary waves can be found in Table 6. Before the collision, the solitary waves propagate at the expected speed. After the collision, it seems that the shapes of these waves do not change much, but these three cases correspond to three different scenarios. The heights and positions of wave crests at the final time $T = 150$ are given in Table 7. In addition, we can estimate the velocities of the left and right waves by picking the positions of the wave crests. We recorded the positions of wave crests at $T = 90$ and $T = 150$, and calculated the average velocities of the waves; see also Table 6. From these data, it can be observed that, after the collision, the solitary waves in case (a) move faster, and the left wave becomes taller while the magnitude of the right wave decays. In case (b), the wave speeds and magnitudes do not change much. In case (c), the solitary waves move slower after the collision, and the left wave becomes shorter while the right wave becomes taller. This observation is consistent with the results reported in [44]. Besides, we expect our method to conserve the discrete total energy, and report the change of the discrete total energy in Fig. 5. It can be observed that the discrete total energy is conserved up to the level of 10^{-12} until the final time $T = 150$.

6.5. *Interaction of two-hump solitary waves with periodic or non-reflecting boundary conditions*

In this subsection, we continue our investigation of the interaction of two solitary waves and test the performance of the proposed methods for interaction of solitary waves with two humps. This test has also been investigated in [43]. The initial condition is given by equations (6.1), which consist of solitary wave with parameters: $x_l = -x_r = -10$, $\Lambda_l = \Lambda_r = 0.2$, $v_l = -v_r = 0.2$. These are two solitary waves with the same two-hump shape but opposite velocities. The computational domain is taken as $[-50, 50]$.

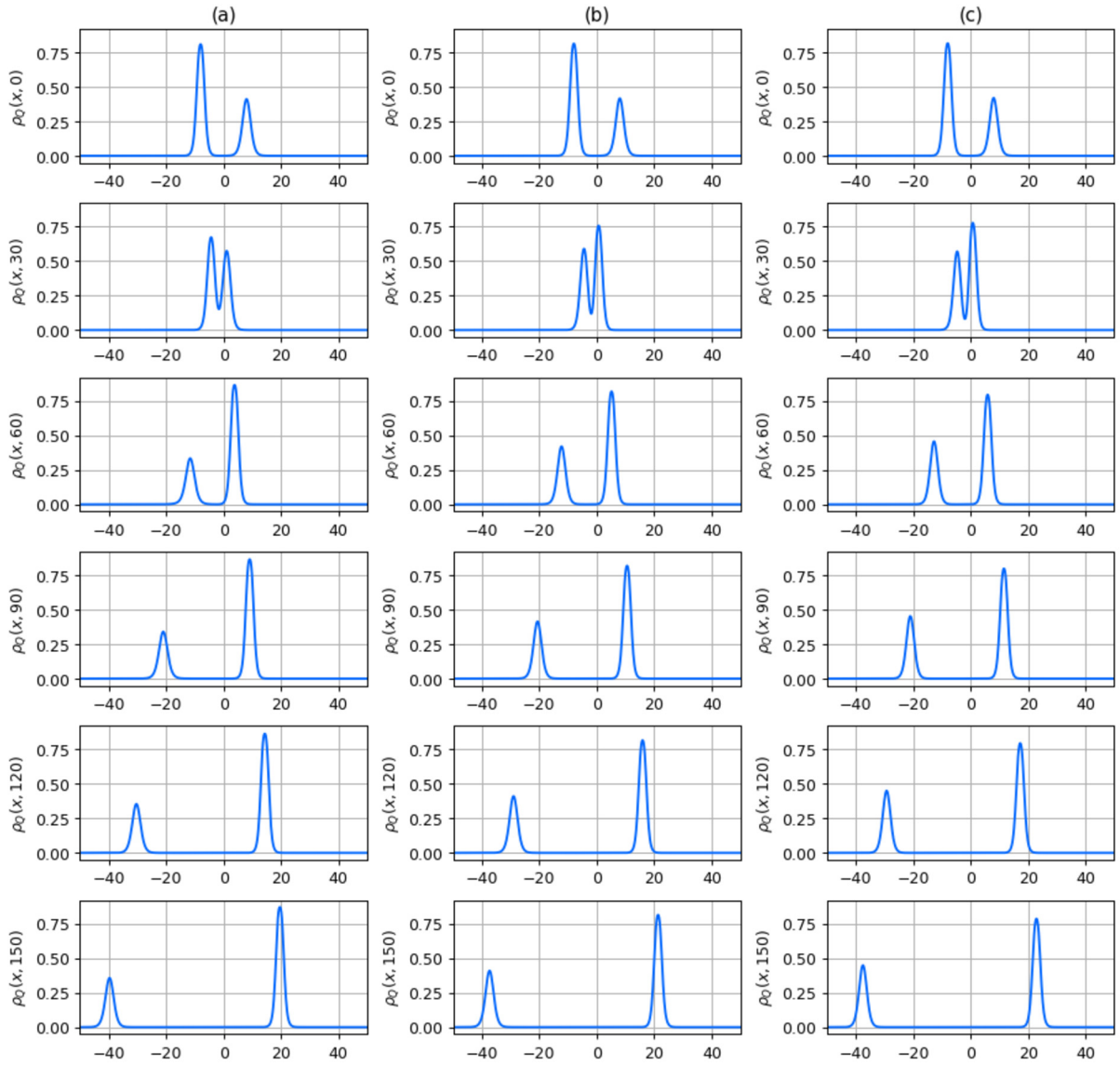

Fig. 4. The evolution of the charge density in Section 6.4 at time $T = 0$, 30, 60, 90, 120 and 150.

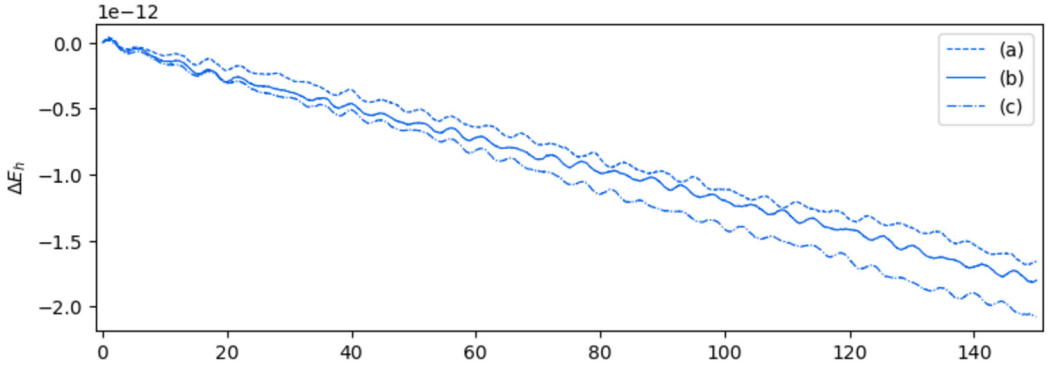

Fig. 5. The change of discrete total energy in Section 6.4.

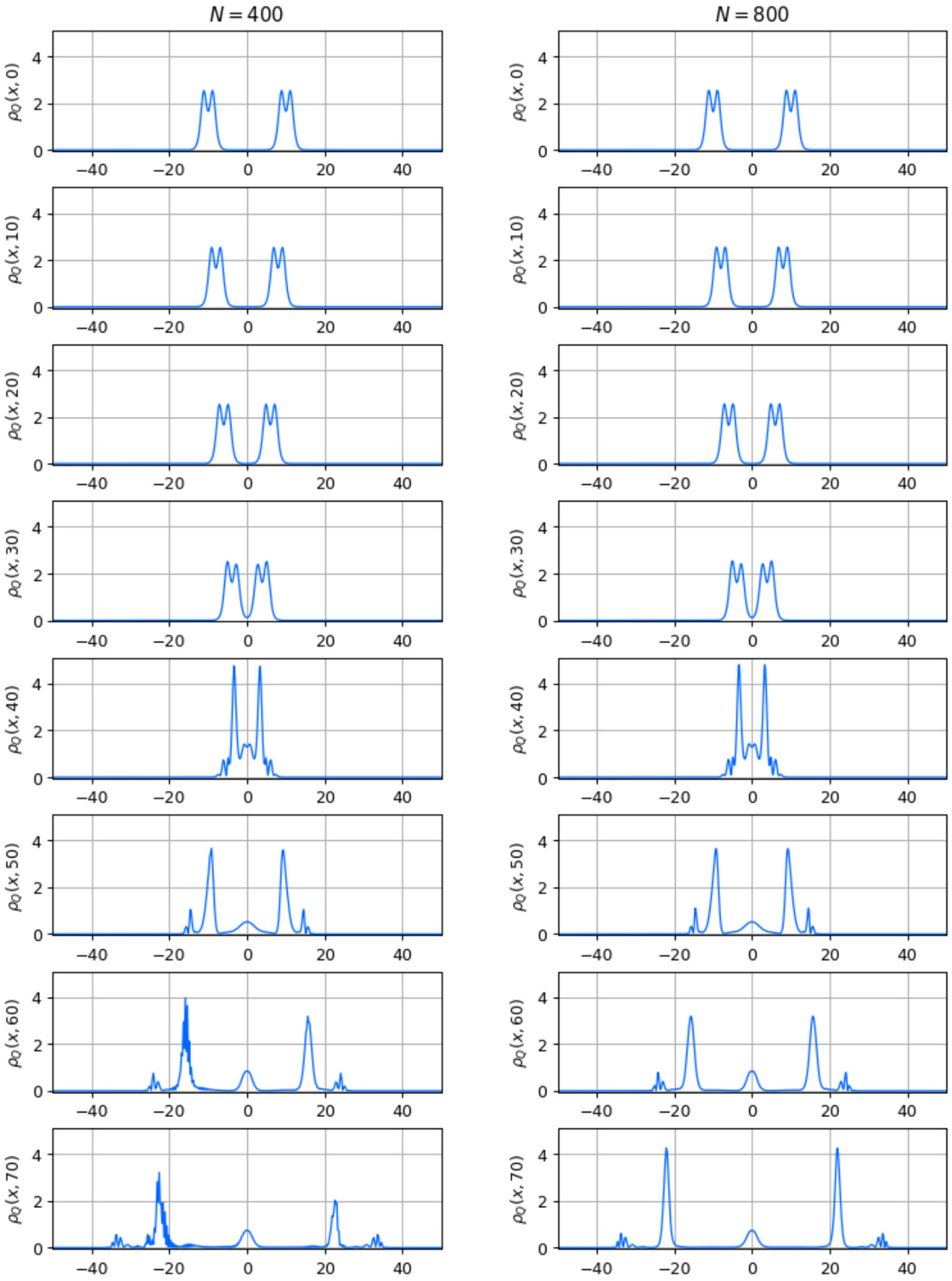

Fig. 6. The evolution of the charge density with periodic boundary condition in Section 6.5.

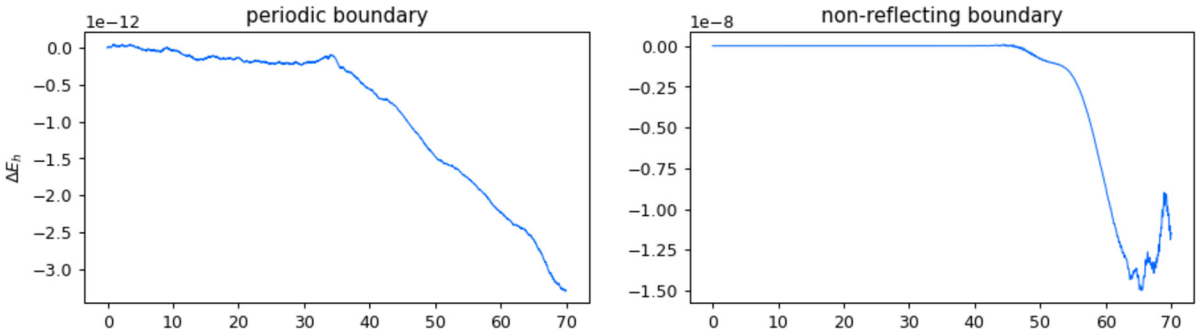

Fig. 7. The change of discrete total energy with $N = 400$ in Section 6.5.

In this example, both the periodic and the commonly used non-reflecting boundary conditions are adopted numerically. The SAV-DG methods with quadratic polynomials ($k = 2$) as finite element basis and the fourth order time integration are used. The charges of numerical solutions with $N = 400$ and $N = 800$ are graphed in Fig. 6. Better resolution can be observed with a refined $N = 800$ mesh. After two initial waves merge, the collapse happens and several oscillating waves are generated. This is different from the interaction of two one-hump waves (as studied in Section 6.4) for which there are still two one-hump waves after merging. As we do not see too much visible difference between numerical solutions with these two types of boundary conditions, only the solutions with periodic boundary conditions are shown in Fig. 6. However, the discrete total energy can only be conserved up to the round-off error level, when the periodic boundary condition is used; please see Fig. 7 for the time history of the change of discrete total energy for both boundary conditions. It can be observed that, with periodic boundary condition, the discrete total energy starts to decay when the collision happens but still maintains at the level of 10^{-12}, while with the non-reflecting boundary condition, the discrete total energy yields an error at the level of 10^{-8}.

7. Conclusion

A family of energy-conserving numerical scheme is proposed for the nonlinear Dirac equation, based on DG spatial methods with the scalar auxiliary variable temporal discretization. We demonstrated that the semi-discrete DG methods enjoy the charge-conserving, energy-conserving and multi-symplectic properties simultaneously. An optimal error estimate is also carried out for the semi-discrete method. This method is coupled with second order or high order SAV time discretization, and rigorous analysis is provided to show that the fully-discrete scheme conserves the discrete global energy exactly. Numerical results are provided to illustrate the order of accuracy of the SAV-DG scheme, its ability to conserve global energy, and the improved approximation in long time simulations.

CRediT authorship contribution statement

Ruize Yang: Conceptualization, Methodology, Software, Validation, Writing, Visualization. **Yulong Xing:** Conceptualization, Methodology, Validation, Writing, Supervision.

Declaration of competing interest

The authors declare that they have no known competing financial interests or personal relationships that could have appeared to influence the work reported in this paper.

References

[1] A. Alvarez, B. Carreras, Interaction dynamics for the solitary waves of a nonlinear Dirac model, Phys. Lett. A 86 (1981) 327–332.
[2] A. Alvarez, P.Y. Kuo, L. Vázquez, The numerical study of a nonlinear one-dimensional Dirac equation, Appl. Math. Comput. 13 (1983) 1–15.
[3] W. Bao, J. Yin, A fourth-order compact time-splitting Fourier pseudospectral method for the Dirac equation, Res. Math. Sci. 6 (2019) 11.
[4] J.L. Bona, H. Chen, O.A. Karakashian, Y. Xing, Conservative discontinuous Galerkin methods for the generalized Korteweg-de Vries equation, Math. Comput. 82 (2013) 1401–1432.
[5] N. Boussaïd, Stable directions for small nonlinear Dirac standing waves, Commun. Math. Phys. 268 (2006) 757–817.
[6] T.J. Bridges, S. Reich, Multi-symplectic integrators: numerical schemes for Hamiltonian PDEs that conserve symplecticity, Phys. Lett. A 284 (2001) 184–193.
[7] J. Cai, J. Shen, Two classes of linearly implicit local energy-preserving approach for general multi-symplectic Hamiltonian PDEs, J. Comput. Phys. 401 (2020) 108975.
[8] T. Candy, Global existence for an L2 critical nonlinear Dirac equation in one dimension, Adv. Differ. Equ. 16 (2011) 643–666.
[9] S.J. Chang, S.D. Ellis, B.W. Lee, Chiral confinement: an exact solution of the massive Thirring model, Phys. Rev. D 11 (1975) 3572–3582.
[10] H. Chen, J. Mao, J. Shen, Optimal error estimates for the scalar auxiliary variable finite-element schemes for gradient flows, Numer. Math. 145 (2020) 167–196.

[11] C.-S. Chou, C.-W. Shu, Y. Xing, Optimal energy conserving local discontinuous Galerkin methods for second-order wave equation in heterogeneous media, J. Comput. Phys. 272 (2014) 88–107.
[12] P. Ciarlet, The Finite Element Method for Elliptic Problem, North-Holland Mathematical Library, 1975.
[13] B. Cockburn, S. Hou, C.-W. Shu, The Runge-Kutta local projection discontinuous Galerkin finite element method for conservation laws. IV. The multidimensional case, Math. Comput. 54 (1990) 545–581.
[14] B. Cockburn, S.-Y. Lin, C.-W. Shu, TVB Runge-Kutta local projection discontinuous Galerkin finite element method for conservation laws III: one-dimensional systems, J. Comput. Phys. 84 (1989) 90–113.
[15] B. Cockburn, C.-W. Shu TVB, Runge-Kutta local projection discontinuous Galerkin finite element method for conservation laws. II. General framework, Math. Comput. 52 (1989) 411–435.
[16] B. Cockburn, C.-W. Shu, The Runge-Kutta local projection P1-discontinuous-Galerkin finite element method for scalar conservation laws, ESAIM: Math. Model. Numer. Anal. 25 (1991) 337–361.
[17] B. Cockburn, C.-W. Shu, The Runge-Kutta discontinuous Galerkin method for conservation laws V: multidimensional systems, J. Comput. Phys. 141 (1998) 199–224.
[18] P. Dirac, The quantum theory of the electron, I, Proc. R. Soc. Lond. A 117 (1928) 610–624.
[19] F. Fillion-Gourdeau, E. Lorin, A. Bandrauk, Numerical solution of the time-dependent Dirac equation in coordinate space without fermion-doubling, Comput. Phys. Commun. 183 (2012) 1403–1415.
[20] Y. Gong, J. Zhao, Q. Wang, Arbitrarily high-order linear energy stable schemes for gradient flow models, J. Comput. Phys. 419 (2020) 109610.
[21] Y. Gong, J. Zhao, Q. Wang, Arbitrarily high-order unconditionally energy stable SAV schemes for gradient flow models, Comput. Phys. Commun. 249 (2020) 107033.
[22] R. Guo, Y. Xing, Optimal energy conserving local discontinuous Galerkin methods for elastodynamics: semi and fully discrete error analysis, J. Sci. Comput. 87 (2021) 13.
[23] R. Hammer, W. Pötz, A. Arnold, A dispersion and norm preserving finite difference scheme with transparent boundary conditions for the Dirac equation in (1+1)D, J. Comput. Phys. 256 (2014) 728–747.
[24] J.L. Hong, C. Li, Multi-symplectic Runge–Kutta methods for nonlinear Dirac equations, J. Comput. Phys. 211 (2006) 448–472.
[25] D. Hou, M. Azaiez, C. Xu, A variant of scalar auxiliary variable approaches for gradient flows, J. Comput. Phys. 395 (2019) 307–332.
[26] Y. Huang, H. Liu, N. Yi, A conservative discontinuous Galerkin method for the Degasperis-Procesi equation, Methods Appl. Anal. 21 (2014) 67–90.
[27] S.Y. Lee, T.K. Kuo, A. Gavrielides, Exact localized solutions of two-dimensional field theories of massive fermions with Fermi interactions, Phys. Rev. D 12 (1975) 2249–2253.
[28] X. Li, Y. Xing, C.-S. Chou, Optimal energy conserving and energy dissipative local discontinuous Galerkin methods for the Benjamin-Bona-Mahony equation, J. Sci. Comput. 83 (2020) 17.
[29] S. Li, X. Li, F. Shi, Time-splitting methods with charge conservation for the nonlinear Dirac equation, Numer. Methods Partial Differ. Equ. 33 (2017) 1582–1602.
[30] X. Liang, A.Q.M. Khaliq, Y. Xing, Fourth order exponential time differencing method with local discontinuous Galerkin approximation for coupled nonlinear Schrödinger equations, Commun. Comput. Phys. 17 (2015) 510–541.
[31] H. Liu, Y. Xing, An invariant preserving discontinuous Galerkin method for the Camassa-Holm equation, SIAM J. Sci. Comput. 38 (2016) A1919–A1934.
[32] H. Liu, N. Yi, A Hamiltonian preserving discontinuous Galerkin method for the generalized Korteweg-de Vries equation, J. Comput. Phys. 321 (2016) 776–796.
[33] H. Liu, P. Yin, On the SAV-DG method for a class of fourth order gradient flows, arXiv:2008.11877.
[34] H. Liu, P. Yin, Energy stable Runge-Kutta discontinuous Galerkin schemes for fourth order gradient flows, arXiv:2101.00152.
[35] S. Machihara, K. Nakanishi, K. Tsugawa, Well-posedness for nonlinear Dirac equations in one dimension, Kyoto J. Math. 50 (2010) 403–451.
[36] P. Mathieu, Compact solitons, bags, and radial excitations, Phys. Rev. D 32 (1985) 3288–3293.
[37] X. Meng, C.-W. Shu, B. Wu, Optimal error estimates for discontinuous Galerkin methods based on upwind-biased fluxes for linear hyperbolic equations, Math. Comput. 85 (2016) 1225–1261.
[38] F.G. Mertens, F. Cooper, N.R. Quintero, S. Shao, A. Khare, A. Saxena, Solitary waves in the nonlinear Dirac equation in the presence of external driving forces, J. Phys. A, Math. Theor. 49 (2016) 065402.
[39] F.G. Mertens, F. Cooper, S. Shao, N.R. Quintero, A. Saxena, A.R. Bishop, Nonlinear Dirac equation solitary waves under a spinor force with different components, J. Phys. A, Math. Theor. 50 (2017) 145201.
[40] J.M. Sanz-Serna, L. Abia, Order conditions for canonical Runge-Kutta schemes, SIAM J. Numer. Anal. 28 (1991) 1081–1096.
[41] S. Selberg, A. Tesfahun, Low regularity well-posedness for some nonlinear Dirac equations in one space dimension, Differ. Integral Equ. 23 (2010) 265–278.
[42] S. Shao, N.R. Quintero, F.G. Mertens, F. Cooper, A. Khare, A. Saxena, Stability of solitary waves in the nonlinear Dirac equation with arbitrary nonlinearity, Phys. Rev. E 90 (2014) 032915.
[43] S. Shao, H. Tang, Interaction for the solitary waves of a nonlinear Dirac model, Phys. Lett. A 345 (2005) 119.
[44] S. Shao, H. Tang, Higher-order accurate Runge-Kutta discontinuous Galerkin methods for a nonlinear Dirac model, Discrete Contin. Dyn. Syst., Ser. B 6 (2006) 623–640.
[45] J. Shen, J. Xu, Convergence and error analysis for the scalar auxiliary variable (SAV) schemes to gradient glows, SIAM J. Numer. Anal. 56 (2018) 2895–2912.
[46] J. Shen, J. Xu, X. Yang, The scalar auxiliary variable (SAV) approach for gradient flows, J. Comput. Phys. 353 (2018) 407–416.
[47] M. Soler, Classical, stable, nonlinear spinor field with positive rest energy, Phys. Rev. D 1 (1970) 2766–2769.
[48] Z. Sun, Y. Xing, On structure-preserving discontinuous Galerkin methods for Hamiltonian partial differential equations: energy conservation and multi-symplecticity, J. Comput. Phys. 419 (2020) 109662.
[49] Z. Sun, Y. Xing, Optimal error estimates of discontinuous Galerkin methods with generalized fluxes for wave equations on unstructured meshes, Math. Comput. 90 (2021) 1741–1772.
[50] B. Thaller, The Dirac Equation, Texts and Monographs in Physics., Springer-Verlag, Berlin, 1992.
[51] J. Werle, Non-linear spinor equations with localized solutions, Lett. Math. Phys. 2 (1977) 109–114.
[52] J. Xu, S. Shao, H. Tang, Numerical methods for nonlinear Dirac equation, J. Comput. Phys. 245 (2013) 131–149.
[53] X. Yang, Linear, first and second-order, unconditionally energy stable numerical schemes for the phase field model of homopolymer blends, J. Comput. Phys. 327 (2016) 294–316.
[54] Y. Zhang, Q. Zhao, Global solution to nonlinear Dirac equation for Gross–Neveu model in $1+1$ dimensions, Nonlinear Anal. 118 (2015) 82–96.
[55] J. Zhao, Q. Wang, X. Yang, Numerical approximations for a phase field dendritic crystal growth model based on the invariant energy quadratization approach, Int. J. Numer. Methods Eng. 110 (2017) 279–300.